

## Electromagnetic structure of octet baryons

Derek B. Leinweber and R. M. Woloshyn

*TRIUMF, 4004 Wesbrook Mall, Vancouver, British Columbia, Canada V6T 2A3*

Terrence Draper

*University of Kentucky, Lexington, Kentucky 40506*

(Received 6 July 1990)

A numerical simulation of quenched QCD on a  $24 \times 12 \times 12 \times 24$  lattice at  $\beta = 5.9$  is used to calculate the electric and magnetic form factors of the baryon octet. General forms of the baryon interpolating fields are considered. Magnetic moments, electric radii, magnetic radii, and magnetic transition moments are extracted from the form factors. The electric properties are found to be consistent with a quark-model picture involving spin-dependent forces. The lattice results for the magnetic properties show a mass and spin dependence of the effective quark moments which is not accounted for in conventional quark models. Lattice calculations underestimate the magnitude of electric radii, magnetic radii, and magnetic moments compared to experimental measurements. The finite volume of the periodic lattice may be responsible for the discrepancies. The pattern of electromagnetic radii in the lattice results are seen to be generally reproduced in the model results that are considered. The only exception is that of  $\Xi^-$  which proves to be a sensitive probe of the quark dynamics. Lattice calculations indicate a positive value for the normalized square magnetic radius in  $\Xi^-$  which contrasts Skyrme model results. Ratios of the magnetic moments allow a more detailed comparison with the experimental measurements. The lattice calculations are seen to better reproduce the experimental ratios than the model calculations.

### I. INTRODUCTION

The nonperturbative regime of quantum chromodynamics has long been an elusive aspect of model-independent calculative techniques. The two most prominent nonperturbative methods which are firmly entrenched in QCD are lattice QCD<sup>1</sup> and the QCD sum-rule approach.<sup>2</sup> The latter approach, while being less numerically intensive, suffers from approximations such as the vacuum-dominance hypothesis, and a perturbative determination of the Wilson coefficients of the operator-product expansion (OPE). Ultimately, the vacuum expectation values of the operators in the OPE are determined phenomenologically. In contrast, lattice QCD allows a calculation of electromagnetic form factors which is parameter-free.

The electromagnetic form factors of hadrons have been studied in lattice QCD over the past five years. Early calculations focused on the pion electric form factor with SU(2) color<sup>3</sup> and later with SU(3) color.<sup>4,5</sup> Calculations of the proton electric form factor followed.<sup>6</sup> More recently both the electric and magnetic form factors of the proton and neutron were calculated<sup>7</sup> from which magnetic moments and electric charge radii were extracted.

In this paper we extend the analysis of Ref. 7 and calculate the electric and magnetic form factors of the octet baryons in lattice QCD at the smallest finite momentum transfer available on our lattice. From these quantities we extract magnetic moments, electric radii, magnetic ra-

dii, and magnetic transition moments. A systematic examination of all the octet baryons reveals the interplay of quark mass effects and spin-dependent forces which are expected in an underlying quark description of baryons. To put our results into perspective, we compare our calculations with experimental measurements where available, with recent quark and Skyrme-model calculations, and with QCD sum-rule calculations.

The interpolating fields coupling to the octet baryons are not unique. The preferred form of the interpolating field is a question that has received some debate<sup>8</sup> in the QCD sum-rule approach. We have completed our analysis using the most general forms of the octet-baryon interpolating fields.<sup>9</sup> These interpolating fields are discussed in Sec. II A. The extraction of baryon mass and electromagnetic form factors proceeds through a calculation of two- and three-point correlation functions. These are discussed at the hadronic level in Sec. II B. The correlation functions at the quark level, calculated with the interpolating fields introduced in Sec. II A, are presented in Sec. II C. Throughout this analysis we employ the lattice techniques introduced in Ref. 7. The important features are briefly discussed in Sec. II D. The results are presented and discussed in Sec. III and summarized in Sec. IV. A detailed tabulation of the results may be found in the Appendix.

In this paper we follow the notation of Sakurai.<sup>10</sup> The Dirac  $\gamma$  matrices are Hermitian and satisfy  $\{\gamma_\mu, \gamma_\nu\} = 2\delta_{\mu\nu}$ , with  $\sigma_{\mu\nu} = (1/2i)[\gamma_\mu, \gamma_\nu]$ .

## II. THEORETICAL FORMALISM

### A. Interpolating fields

The commonly used interpolating field for the proton in lattice calculations has the form

$$\chi_1^p(x) = \epsilon^{abc} [u^{aT}(x) C \gamma_5 d^b(x)] u^c(x), \quad (2.1)$$

where  $C$  is the charge-conjugation matrix and Dirac indices have been suppressed. In the sum-rule approach it is common to find linear combinations of this interpolating field and

$$\chi_2^p(x) = \epsilon^{abc} [u^{aT}(x) C d^b(x)] \gamma_5 u^c(x), \quad (2.2)$$

which vanishes in the nonrelativistic limit. With the use of the Fierz relations, the combination of the above two

interpolating fields with a relative minus sign may be written

$$\chi^p(x) = \epsilon^{abc} [u^{aT}(x) C \gamma_\rho u^b(x)] \gamma_5 \gamma_\rho d^c(x), \quad (2.3)$$

giving the proton interpolating field often found in sum-rule calculations.<sup>11</sup>

In this analysis we will consider both interpolating fields introduced in (2.1) and (2.2) and their interference terms such that any linear combination of these interpolating fields may be investigated. Interpolating fields for the remaining members of the baryon octet in which there is a doubly occurring quark may be obtained from (2.1) and (2.2) by replacing the  $u$ - and  $d$ -quark fields in these equations with  $u$ -,  $d$ -, or  $s$ -quark fields appropriately. For  $\Sigma^0$  and  $\Lambda$  interpolating fields where  $u$ ,  $d$ , and  $s$  quarks each occur once, we consider

$$\chi_1^{\Sigma^0} = \epsilon^{abc} (\frac{1}{2})^{1/2} \{ [u^{aT}(x) C \gamma_5 s^b(x)] d^c(x) + [d^{aT}(x) C \gamma_5 s^b(x)] u^c(x) \}, \quad (2.4a)$$

$$\chi_2^{\Sigma^0} = \epsilon^{abc} (\frac{1}{2})^{1/2} \{ [u^{aT}(x) C s^b(x)] \gamma_5 d^c(x) + [d^{aT}(x) C s^b(x)] \gamma_5 u^c(x) \}, \quad (2.4b)$$

for  $\Sigma^0$  and

$$\chi_1^\Lambda(x) = \epsilon^{abc} (\frac{1}{6})^{1/2} \{ 2[u^{aT}(x) C \gamma_5 d^b(x)] s^c(x) + [u^{aT}(x) C \gamma_5 s^b(x)] d^c(x) - [d^{aT}(x) C \gamma_5 s^b(x)] u^c(x) \}, \quad (2.5a)$$

$$\chi_2^\Lambda(x) = \epsilon^{abc} (\frac{1}{6})^{1/2} \{ 2[u^{aT}(x) C d^b(x)] \gamma_5 s^c(x) + [u^{aT}(x) C s^b(x)] \gamma_5 d^c(x) - [d^{aT}(x) C s^b(x)] \gamma_5 u^c(x) \}, \quad (2.5b)$$

for the octet  $\Lambda$ . Note that the leading term in the  $\Lambda$  interpolating fields changes sign if one uses the transpose of the quantity in square brackets to exchange the  $u$  and  $d$  quarks. Hence the isospin antisymmetry of the  $u$ - $d$  sector is evident in this interpolating field. To complete the analysis of low-lying  $J = \frac{1}{2}$  baryons we also consider the flavor-singlet interpolating field

$$\chi^{\Lambda_s}(x) = \epsilon^{abc} \epsilon_{uds} [u^{aT}(x) C \gamma_5 d^b(x)] s^c(x). \quad (2.6)$$

Using the transpose of the terms in square brackets, (2.6) may be written

$$\chi^{\Lambda_s}(x) = -2\epsilon^{abc} \{ -[u^{aT}(x) C \gamma_5 d^b(x)] s^c(x) + [u^{aT}(x) C \gamma_5 s^b(x)] d^c(x) - [d^{aT}(x) C \gamma_5 s^b(x)] u^c(x) \}, \quad (2.7)$$

which has a structure very similar to the octet interpolating field of (2.5a) with the exception of the coefficient of the first term. Since SU(3) flavor is broken it may be interesting to investigate an interpolating field made up of the terms common to both the octet and singlet interpolating fields. Such an interpolating field would not make any assumptions on the flavor symmetry of the quarks composing  $\Lambda$ . We define

$$\chi^{\Lambda_c}(x) = \epsilon^{abc} (\frac{1}{2})^{1/2} \{ [u^{aT}(x) C \gamma_5 s^b(x)] d^c(x) - [d^{aT}(x) C \gamma_5 s^b(x)] u^c(x) \}. \quad (2.8)$$

In this interpolating field the antisymmetric isospin symmetry of the  $u$ - $d$  sector is evident and corresponds to the symmetric interpolating field of  $\Sigma^0$  in (2.4a).

### B. Correlation functions at the hadronic level

The extraction of baryon mass and electromagnetic form factors proceeds through the calculation of the ensemble average (denoted  $\langle \dots \rangle$ ) of two- and three-point Green's functions. The two-point function is defined as

$$\langle G^{BB}(t; \mathbf{p}, \Gamma) \rangle = \sum_{\mathbf{x}} e^{i\mathbf{p} \cdot \mathbf{x}} \Gamma^{\beta\alpha} \langle \Omega | T(\chi^\alpha(x) \bar{\chi}^\beta(0)) | \Omega \rangle. \quad (2.9)$$

Here  $\Omega$  represents the QCD vacuum,  $\Gamma$  is a  $4 \times 4$  matrix in Dirac space and  $\alpha, \beta$  are Dirac indices. At the hadronic level we insert a complete set of states  $|B, p, s\rangle$  and define

$$\langle \Omega | \chi(0) | B, p, s \rangle = Z_B \left[ \frac{M}{E_p} \right]^{1/2} u(p, s), \quad (2.10)$$

where  $Z$  represents the coupling strength of  $\chi(0)$  to baryon  $B$ , and  $E_p = (\mathbf{p}^2 + M^2)^{1/2}$ . For large Euclidean time

$$\langle G^{BB}(t; \mathbf{p}, \Gamma) \rangle \simeq \frac{Z_B^2}{2E_p} e^{-E_p t} \text{tr}[\Gamma(-i\gamma \cdot p + M)] . \quad (2.11)$$

Similarly the three-point Green's function for the electromagnetic current,  $j^\mu(x)$ , is defined as

$$\langle G^{Bj^\mu B}(t_2, t_1; \mathbf{p}', \mathbf{p}; \Gamma) \rangle = \sum_{x_2, x_1} e^{-i\mathbf{p}' \cdot \mathbf{x}_2} e^{+i(\mathbf{p}' - \mathbf{p}) \cdot \mathbf{x}_1} \Gamma^{\beta\alpha} \langle \Omega | T(\chi^\alpha(x_2) j^\mu(x_1) \bar{\chi}^\beta(0)) | \Omega \rangle . \quad (2.12)$$

For large Euclidean time separations  $t_2 - t_1 \gg 1$  and  $t_1 \gg 1$  the three-point function at the hadronic level takes the limit

$$\langle G^{Bj^\mu B}(t_2, t_1; \mathbf{p}', \mathbf{p}; \Gamma) \rangle = \sum_{s, s'} e^{-E_p(t_2 - t_1)} e^{-E_p t_1} \Gamma^{\beta\alpha} \langle \Omega | \chi^\alpha | p', s' \rangle \langle p', s' | j^\mu | p, s \rangle \langle p, s | \bar{\chi}^\beta | \Omega \rangle . \quad (2.13)$$

The matrix element of the electromagnetic current has the general form

$$\langle p', s' | j^\mu | p, s \rangle = \left[ \frac{M^2}{E_p E_{p'}} \right]^{1/2} \bar{u}(p', s') \left[ F_1(q^2) \gamma^\mu - F_2(q^2) \sigma^{\mu\nu} \frac{q^\nu}{2M} \right] u(p, s) , \quad (2.14)$$

where  $q = p' - p$ . To eliminate the time dependence of the three-point functions we construct the ratio

$$\begin{aligned} R(t_2, t_1; \mathbf{p}', \mathbf{p}; \Gamma, \Gamma'; \mu) &= \left[ \frac{\langle G^{Bj^\mu B}(t_2, t_1; \mathbf{p}', \mathbf{p}; \Gamma) \rangle \langle G^{Bj^\mu B}(t_2, t_1; -\mathbf{p}, -\mathbf{p}'; \Gamma') \rangle}{\langle G^{BB}(t_2; \mathbf{p}'; \Gamma') \rangle \langle G^{BB}(t_2; -\mathbf{p}; \Gamma') \rangle} \right]^{1/2} \\ &\rightarrow \left[ \frac{E_p + M}{2E_p} \right]^{1/2} \left[ \frac{E_{p'} + M}{2E_{p'}} \right]^{1/2} \bar{R}(\mathbf{p}', \mathbf{p}; \Gamma, \Gamma'; \mu) , \end{aligned} \quad (2.15)$$

where we have defined the reduced ratio  $\bar{R}(\mathbf{p}', \mathbf{p}; \Gamma, \Gamma'; \mu)$ . The Sachs forms for the electromagnetic form factors

$$\mathcal{G}_E(q^2) = F_1(q^2) - \frac{q^2}{(2M)^2} F_2(q^2) , \quad (2.16a)$$

$$\mathcal{G}_M(q^2) = F_1(q^2) + F_2(q^2) , \quad (2.16b)$$

may be extracted through an appropriate choice of  $\Gamma$  and  $\Gamma'$ . A straightforward calculation reveals

$$\bar{R}(\mathbf{q}, \mathbf{0}; \Gamma_4, \Gamma_4, 4) = \mathcal{G}_E(q^2) , \quad (2.17a)$$

$$\bar{R}(\mathbf{q}, \mathbf{0}; \Gamma_j, \Gamma_4, k) = \frac{\mathcal{G}_M(q^2) |\epsilon_{ijk} q^i|}{(E_q + M)} , \quad (2.17b)$$

$$\bar{R}(\mathbf{q}, \mathbf{0}; \Gamma_4, \Gamma_4, k) = \frac{\mathcal{G}_E(q^2) |q^k|}{(E_q + M)} , \quad (2.17c)$$

where

$$\Gamma_j = \frac{1}{2} \begin{bmatrix} \sigma_j & 0 \\ 0 & 0 \end{bmatrix}, \quad \Gamma_4 = \frac{1}{2} \begin{bmatrix} I & 0 \\ 0 & 0 \end{bmatrix} . \quad (2.18)$$

For large time separations  $t_2 - t_1 \gg 1$  and  $t_1 \gg 1$  these ratios are constant in time and are proportional to the electromagnetic form factors.

For the magnetic transition moment of  $\Sigma^0 \rightarrow \Lambda \gamma$  the matrix element of the electromagnetic current may be written

$$\langle p', s' | j^\mu | p, s \rangle = \left[ \frac{M^2}{E_p E_{p'}} \right]^{1/2} \bar{u}(p', s') \left[ F_1(q^2) \left[ \gamma^\mu - i \frac{M' - M}{q^2} q^\mu \right] - F_2(q^2) \sigma^{\mu\nu} \frac{q^\nu}{M + M'} \right] u(p, s) , \quad (2.19)$$

satisfying gauge invariance and parity conservation. By selecting this construction of the current matrix element, the magnetic transition moment has the same form as the Sachs form of  $\mathcal{G}_M(q^2)$  indicated in (2.16b). Similarly, (2.17b) allows the extraction of the magnetic transition moment from the following ratio of lattice correlation functions:

$$R(t_2, t_1; \mathbf{p}', \mathbf{p}; \Gamma, \Gamma'; \mu) = \left[ \frac{\langle G^{\Lambda j^\mu \Sigma^0}(t_2, t_1; \mathbf{p}', \mathbf{p}; \Gamma) \rangle \langle G^{\Sigma^0 j^\mu \Lambda}(t_2, t_1; -\mathbf{p}, -\mathbf{p}'; \Gamma') \rangle}{\langle G^{\Lambda \Lambda}(t_2; \mathbf{p}'; \Gamma') \rangle \langle G^{\Sigma^0 \Sigma^0}(t_2; -\mathbf{p}; \Gamma') \rangle} \right]^{1/2} . \quad (2.20)$$

### C. Correlation functions at the quark level

Calculations at the quark level proceed by inserting the interpolating fields introduced in (2.1) through (2.8) into the two- and three-point functions defined in (2.9) and (2.12), respectively. For the octet baryons it is convenient to define the correlation function

$$\mathcal{F}(S_{f_1}, S_{f_2}, S_{f_3}) = \epsilon^{abc} \epsilon^{a'b'c'} \{ S_{f_1}^{aa'}(x, 0) \text{tr}[S_{f_2}^{bb'}(x, 0) S_{f_3}^{cc'T}(x, 0)] + S_{f_1}^{aa'}(x, 0) S_{f_3}^{cc'T}(x, 0) S_{f_2}^{bb'}(x, 0) \} . \quad (2.21)$$

where  $S^{aa'}(x, 0) = T\{q^a(x), \bar{q}^{a'}(0)\}$  and  $f_1, f_2, f_3$  are flavor labels. For  $u$ -quark fields we denote  $S_u^{aa'}(x, 0) = T\{u^a(x), \bar{u}^{a'}(0)\}$  and similarly for  $d$ - and  $s$ -quark fields. For the proton interpolating field  $\chi_1^p$  of (2.1) the two-point function may be written

$$G_1^{pp}(t, \mathbf{p}; \Gamma) = \sum_{\mathbf{x}} e^{-i\mathbf{p}\cdot\mathbf{x}} \text{tr}[\Gamma \mathcal{F}(S_u, S_u, \tilde{C} S_d \tilde{C}^{-1})] , \quad (2.22)$$

where  $\tilde{C} = C\gamma_5$ . Similarly the two-point function corresponding to  $\chi_2^p$  may be written in the form

$$G_2^{pp}(t, \mathbf{p}; \Gamma) = \sum_{\mathbf{x}} e^{-i\mathbf{p}\cdot\mathbf{x}} \text{tr}[\Gamma \mathcal{F}(\gamma_5 S_u \gamma_5, \gamma_5 S_u \gamma_5, \tilde{C} S_d \tilde{C}^{-1})] , \quad (2.23)$$

The interference contributions of these two interpolating fields are

$$G_1^{pp}(t, \mathbf{p}; \Gamma) = \sum_{\mathbf{x}} e^{-i\mathbf{p}\cdot\mathbf{x}} \text{tr}\{ -\Gamma [\mathcal{F}(S_u \gamma_5, S_u \gamma_5, \tilde{C} S_d \tilde{C}^{-1}) + \mathcal{F}(\gamma_5 S_u, \gamma_5 S_u, \tilde{C} S_d \tilde{C}^{-1})] \} , \quad (2.24)$$

The correlation functions of the other five members of the baryon octet in which there is a doubly occurring quark field may be obtained from the above three equations with the appropriate substitutions of quark fields. For example the replacement of all occurrences of  $u$ -quark fields with  $s$ -quark fields results in the correlation functions for  $\Xi^-$ . For  $\Sigma^0$  the correlation functions correspond to the interpolating fields of (2.4a) and (2.4b) are

$$G_1^{\Sigma^0}(t, \mathbf{p}; \Gamma) = \frac{1}{2} \sum_{\mathbf{x}} e^{-i\mathbf{p}\cdot\mathbf{x}} \text{tr}\{ \Gamma [\mathcal{F}(S_d, S_u, \tilde{C} S_s \tilde{C}^{-1}) + \mathcal{F}(S_u, S_d, \tilde{C} S_s \tilde{C}^{-1})] \} , \quad (2.25a)$$

$$G_2^{\Sigma^0}(t, \mathbf{p}; \Gamma) = \frac{1}{2} \sum_{\mathbf{x}} e^{-i\mathbf{p}\cdot\mathbf{x}} \text{tr}\{ \Gamma [\mathcal{F}(\gamma_5 S_d \gamma_5, \gamma_5 S_u \gamma_5, \tilde{C} S_s \tilde{C}^{-1}) + F(\gamma_5 S_u \gamma_5, \gamma_5 S_d \gamma_5, \tilde{C} S_s \tilde{C}^{-1})] \} , \quad (2.25b)$$

respectively. The isospin symmetry of the  $u$  and  $d$  quarks is apparent in these equations. On comparing with the correlation functions of  $\Sigma^+$  and  $\Sigma^-$  it becomes clear that (2.5) is an average of the charged  $\Sigma$  correlation functions. The correlation function corresponding to the interpolating field of (2.5a) for the octet  $\Lambda$  denoted  $\Lambda_8$  is

$$\begin{aligned} G_1^{\Lambda_8}(t, \mathbf{p}; \Gamma) = & \frac{1}{6} \sum_{\mathbf{x}} e^{-i\mathbf{p}\cdot\mathbf{x}} \text{tr}\{ \Gamma [2\mathcal{F}(S_s, S_d, \tilde{C} S_u \tilde{C}^{-1}) + 2\mathcal{F}(S_s, S_u, \tilde{C} S_d \tilde{C}^{-1}) \\ & + 2\mathcal{F}(S_d, S_s, \tilde{C} S_u \tilde{C}^{-1}) + 2\mathcal{F}(S_u, S_s, \tilde{C} S_d \tilde{C}^{-1}) \\ & - \mathcal{F}(S_d, S_u, \tilde{C} S_s \tilde{C}^{-1}) - \mathcal{F}(S_u, S_d, \tilde{C} S_s \tilde{C}^{-1})] \} , \end{aligned} \quad (2.26)$$

and similarly for the interpolating field of (2.5b). Note that in the limit of SU(3)-flavor symmetry all correlation functions introduced to this point simplify to the proton two-point functions. The two-point correlation function of  $\Lambda_C$  is best illustrated with the use of

$$\bar{\mathcal{F}}(S_{f_1}, S_{f_2}, S_{f_3}) = \epsilon^{abc} \epsilon^{a'b'c'} \{ S_{f_1}^{aa'}(x, 0) \text{tr}[S_{f_2}^{bb'}(x, 0) S_{f_3}^{cc'T}(x, 0)] - S_{f_1}^{aa'}(x, 0) S_{f_3}^{cc'T}(x, 0) S_{f_2}^{bb'}(x, 0) \} , \quad (2.27)$$

where the relative sign of the two terms in  $\mathcal{F}$  has been changed. With this definition the correlation function of  $\Lambda_C$  is

$$G^{\Lambda_C}(t, \mathbf{p}; \Gamma) = \frac{1}{2} \sum_{\mathbf{x}} e^{-i\mathbf{p}\cdot\mathbf{x}} \text{tr}\{ \Gamma [\bar{\mathcal{F}}(S_d, S_u, \tilde{C} S_s \tilde{C}^{-1}) + \bar{\mathcal{F}}(S_u, S_d, \tilde{C} S_s \tilde{C}^{-1})] \} . \quad (2.28)$$

The flavor-singlet correlation function is

$$\begin{aligned} G^{\Lambda_S}(t, \mathbf{p}; \Gamma) = & \sum_{\mathbf{x}} e^{-i\mathbf{p}\cdot\mathbf{x}} \text{tr}\{ \Gamma [\gamma_5 S_s^{aa'} \tilde{C} S_d^{cc'T} \tilde{C}^{-1} S_u^{bb'} \gamma_5 + \gamma_5 S_u^{aa'} \tilde{C} S_d^{cc'T} \tilde{C}^{-1} S_s^{bb'} \gamma_5 + \gamma_5 S_s^{aa'} \tilde{C} S_u^{cc'T} \tilde{C}^{-1} S_d^{bb'} \gamma_5 \\ & + \gamma_5 S_d^{aa'} \tilde{C} S_u^{cc'T} \tilde{C}^{-1} S_s^{bb'} \gamma_5 + \gamma_5 S_u^{aa'} \tilde{C} S_s^{cc'T} \tilde{C}^{-1} S_d^{bb'} \gamma_5 + \gamma_5 S_d^{aa'} \tilde{C} S_s^{cc'T} \tilde{C}^{-1} S_u^{bb'} \gamma_5 \\ & - \gamma_5 S_s^{aa'} \gamma_5 \text{tr}(S_d^{bb'} \tilde{C} S_u^{cc'T} \tilde{C}^{-1}) - \gamma_5 S_u^{aa'} \gamma_5 \text{tr}(S_s^{bb'} \tilde{C} S_d^{cc'T} \tilde{C}^{-1}) \\ & - \gamma_5 S_d^{aa'} \gamma_5 \text{tr}(S_u^{bb'} \tilde{C} S_s^{cc'T} \tilde{C}^{-1})] \} . \end{aligned} \quad (2.29)$$

The SU(3)-flavor-singlet symmetry of  $u$ -,  $d$ -, and  $s$ -quark fields is displayed in this equation.

The three-point functions have the same structure as the two-point correlation functions listed in (2.22) through (2.29). In constructing the three-point functions, each of the three propagators  $S$  in the two-point functions is replaced one at a time by  $\hat{S}$  denoting the propagation of a quark in the presence of the electromagnetic current  $j^\mu$ . Rather than write out all of these correlation functions which are three times the length of the two-point correlation functions, we simply illustrate the three-point function structure by writing out the proton three-point correlation function corresponding to the interpolating field of (2.1) in detail.

$$\begin{aligned}
G_1^{pj^{\mu p}}(t_2, t_1; \mathbf{p}', \mathbf{p}; \Gamma) = & \sum_{x_2} e^{-i\mathbf{p}' \cdot \mathbf{x}_2} \epsilon^{abc} \epsilon^{a'b'c'} \text{tr} \{ \Gamma \{ \hat{S}_u^{aa'}(x_2, 0; t_1, \mathbf{q}, \mu) \text{tr} [ S_u^{bb'}(x_2, 0) \tilde{C} S_d^{cc'T}(x_2, 0) \tilde{C}^{-1} ] \\
& + S_u^{aa'}(x_2, 0) \text{tr} [ \hat{S}_u^{bb'}(x_2, 0; t_1, \mathbf{q}, \mu) \tilde{C} S_d^{cc'T}(x_2, 0) \tilde{C}^{-1} ] \\
& + S_u^{aa'}(x_2, 0) \text{tr} [ S_u^{bb'}(x_2, 0) \tilde{C} \hat{S}_d^{cc'T}(x_2, 0; t_1, \mathbf{q}, \mu) \tilde{C}^{-1} ] \\
& + \hat{S}_u^{aa'}(x_2, 0; t_1, \mathbf{q}, \mu) \tilde{C} S_d^{cc'T}(x_2, 0) \tilde{C}^{-1} S_u^{bb'}(x_2, 0) \\
& + S_u^{aa'}(x_2, 0) \tilde{C} \hat{S}_d^{cc'T}(x_2, 0; t_1, \mathbf{q}, \mu) \tilde{C}^{-1} S_u^{bb'}(x_2, 0) \\
& + S_u^{aa'}(x_2, 0) \tilde{C} S_d^{cc'T}(x_2, 0) \tilde{C}^{-1} \hat{S}_u^{bb'}(x_2, 0; t_1, \mathbf{q}, \mu) \} \} . \quad (2.30)
\end{aligned}$$

The  $t_1$ ,  $\mathbf{q}$ , and  $\mu$  dependence of  $\hat{S}$  has been shown explicitly.

For the  $\Sigma^0 \rightarrow \Lambda \gamma$  transition we require two three-point correlation functions as illustrated in (2.20). For the full octet  $\Lambda$  interpolating field of (2.5a) the three-point correlation functions may be written

$$\begin{aligned}
G_1^{\Lambda_8 j^{\mu \Sigma^0}}(t_2, t_1; \mathbf{p}', \mathbf{p}; \Gamma) = & (\frac{1}{12})^{1/2} \sum_{x_2} e^{-i\mathbf{p}' \cdot \mathbf{x}_2} \text{tr} \{ \Gamma [ 2\mathcal{F}(\hat{S}_s, S_d, \tilde{C} S_u \tilde{C}^{-1}) - 2\mathcal{F}(\hat{S}_s, S_u, \tilde{C} S_d \tilde{C}^{-1}) \\
& + \mathcal{F}(S_d, S_u, \tilde{C} \hat{S}_s \tilde{C}^{-1}) - \mathcal{F}(S_u, S_d, \tilde{C} \hat{S}_s \tilde{C}^{-1}) + \dots ] \} \quad (2.31a)
\end{aligned}$$

and

$$\begin{aligned}
G_1^{\Sigma^0 j^{\mu \Lambda_8}}(t_2, t_1; \mathbf{p}', \mathbf{p}; \Gamma) = & (\frac{1}{12})^{1/2} \sum_{x_2} e^{-i\mathbf{p}' \cdot \mathbf{x}_2} \text{tr} \{ \Gamma [ 2\mathcal{F}(S_d, \hat{S}_s, \tilde{C} S_u \tilde{C}^{-1}) - 2\mathcal{F}(S_u, \hat{S}_s, \tilde{C} S_d \tilde{C}^{-1}) \\
& + \mathcal{F}(S_u, S_d, \tilde{C} \hat{S}_s \tilde{C}^{-1}) - \mathcal{F}(S_d, S_u, \tilde{C} \hat{S}_s \tilde{C}^{-1}) + \dots ] \} , \quad (2.31b)
\end{aligned}$$

where the ellipsis indicates the terms in which  $u$  and  $d$  quarks interact with the electromagnetic current. For the more simple interpolating field of  $\Lambda_C$  the three-point correlation functions are

$$G_1^{\Lambda_C j^{\mu \Sigma^0}}(t_2, t_1; \mathbf{p}', \mathbf{p}; \Gamma) = \frac{1}{2} \sum_{x_2} e^{-i\mathbf{p}' \cdot \mathbf{x}_2} \text{tr} \{ \Gamma [ \mathcal{F}(S_d, S_u, \tilde{C} \hat{S}_s \tilde{C}^{-1}) - \mathcal{F}(S_u, S_d, \tilde{C} \hat{S}_s \tilde{C}^{-1}) + \dots ] \} \quad (2.32a)$$

and

$$G_1^{\Sigma^0 j^{\mu \Lambda_C}}(t_2, t_1; \mathbf{p}', \mathbf{p}; \Gamma) = \frac{1}{2} \sum_{x_2} e^{-i\mathbf{p}' \cdot \mathbf{x}_2} \text{tr} \{ \Gamma [ \bar{\mathcal{F}}(S_d, S_u, \tilde{C} \hat{S}_s \tilde{C}^{-1}) - \bar{\mathcal{F}}(S_u, S_d, \tilde{C} \hat{S}_s \tilde{C}^{-1}) + \dots ] \} . \quad (2.32b)$$

In the following calculations we assume an SU(2)-isospin symmetry for the quark fields. In this case the two-point functions corresponding to (2.31) and (2.32) vanish as required. Furthermore the strange quark does not participate in the electromagnetic decay of  $\Sigma^0$ ; the contribution of the terms of (2.31) and (2.32) in which the strange quark interacts with the electromagnetic current vanishes under SU(2) symmetry.

#### D. Lattice techniques

Here we briefly summarize the lattice techniques used in the following calculations.<sup>7</sup> We use Wilson's formulation for both the gauge  $\mathcal{S}_G$  and fermionic  $\mathcal{S}_F$  action:

$$\begin{aligned}
\mathcal{S}_F(\{U\}) = & \bar{\psi} M(\{U\}) \psi \\
= & \sum_{x,f} \bar{\psi}^f(x) \psi^f(x) - \sum_{x,\mu,f} \kappa_f (\bar{\psi}^f(x) (1 - \gamma^\mu) U^\mu(x) \psi^f(x + \hat{\mu}) + \bar{\psi}^f(x + \hat{\mu}) (1 + \gamma^\mu) U^{\mu\dagger}(x) \psi^f(x)) , \quad (2.33)
\end{aligned}$$

where  $f$  sums over the flavors of the quarks, and the quark propagator  $S = M^{-1}$ . SU(2) isospin symmetry is enforced by equating the Wilson hopping parameters  $\kappa_u = \kappa_d = \kappa$ . We select three values of  $\kappa$ , which we denote  $\kappa_1 = 0.152$ ,  $\kappa_2 = 0.154$ , and  $\kappa_3 = 0.156$ , and extrapolate the  $u$ - $d$  quark sector to the chiral limit. To account for the relatively heavy strange quark we fix  $\kappa_s = \kappa_1$ , the smallest of the three values of  $\kappa$  considered. This allows the rather acceptable extrapolation of the light quarks to the chiral limit through values of  $\kappa$  less than or equal to  $\kappa_s$ . Our calculations of baryon mass indicate that this selection of  $\kappa_s$  gives a reasonable description of the strange-quark dynamics.

The electromagnetic current, conserved on the lattice, is derived from the fermionic action  $\mathcal{S}_F$  by the Noether procedure:

$$\hat{S}_f(x_2, 0; t_1, \mathbf{q}, \mu) = Q_f \sum_{x_1} e^{+i\mathbf{q}\cdot x_1} \kappa (S(x_2, x_1 + \hat{\mu})(1 + \gamma^\mu)U^{\mu\dagger}(x_1)S(x_1, 0) - S(x_2, x_1)(1 - \gamma^\mu)U^\mu(x_1)S(x_1 + \hat{\mu}, 0)) , \quad (2.35)$$

and is calculated using the sequential source technique.<sup>12,13</sup>

The two- and three-point correlation functions are defined as averages over an infinite ensemble of equilibrium gauge field configurations, but are approximated by an average over a finite number of configurations. To minimize the noise in the results, we exploit the parity of the correlation functions

$$G(\mathbf{p}', \mathbf{p}, \mathbf{q}; \Gamma) = s_p G(-\mathbf{p}', -\mathbf{p}, -\mathbf{q}; \Gamma) , s_p = \pm 1 , \quad (2.36)$$

and calculate them for both  $\mathbf{p}, \mathbf{p}', \mathbf{q}$  and  $-\mathbf{p}, -\mathbf{p}', -\mathbf{q}$ . While this requires an extra matrix inversion to determine  $\hat{S}(x_2, 0; t_1, -\mathbf{q}, \mu)$  the calculation is worthwhile. By determining the correlation functions with both sets of momenta, the ratio of (2.15) is determined with a substantial reduction in the statistical uncertainties.<sup>14</sup>

The link variables  $\{U\}$  and  $\{U^*\}$  are gauge field configurations of equal weight, and therefore we account for both configurations in calculating the correlation functions. With the fermion matrix property

$$M(\{U^*\}) = (\bar{C}M(\{U\})\bar{C}^{-1})^* , \quad (2.37)$$

it follows that

$$S(x, 0; \{U^*\}) = (\bar{C}S(x, 0; \{U\})\bar{C}^{-1})^* , \quad (2.38a)$$

$$\hat{S}(x, 0; t, \mathbf{q}, \mu; \{U^*\}) = (\bar{C}\hat{S}(x, 0; t, -\mathbf{q}, \mu; \{U\})\bar{C}^{-1})^* , \quad (2.38b)$$

and therefore the correlation functions are real provided

$$\Gamma = s_C (\bar{C}\Gamma\bar{C}^{-1})^* \text{ and } s_C = s_p . \quad (2.39)$$

These conditions are satisfied with the selections for  $\Gamma$  indicated in (2.17a), (2.17b) and (2.18). In summary, the inclusion of both  $\{U\}$  and  $\{U^*\}$  configurations in the calculation of the correlation functions allows an unbiased estimate of the ensemble average properties which has

$$j^\mu(x) = \sum_f Q_f \kappa_f (\bar{\psi}^f(x + \hat{\mu})(1 + \gamma^\mu)U^{\mu\dagger}(x)\psi^f(x) - \bar{\psi}^f(x)(1 - \gamma^\mu)U^\mu(x)\psi^f(x + \hat{\mu})) , \quad (2.34)$$

where  $Q_f$  is the charge of the quark of flavor  $f$ . In the limit of the lattice spacing  $a \rightarrow 0$ ,  $j^\mu$  reduces to the continuum current. This current is exactly conserved on the lattice and therefore no renormalization is required to relate the lattice matrix elements to those in the continuum.

The quark propagator coupled with momentum  $\mathbf{q}$  to  $j^\mu$  is

significantly smaller fluctuations.

Twenty-eight quenched gauge configurations are generated by the Cabibbo-Marinari<sup>15</sup> pseudo-heat-bath method on a  $24 \times 12 \times 12 \times 24$  periodic lattice at  $\beta = 5.9$ . Dirichlet or fixed boundary conditions are used in the time direction. Configurations are selected after 5000 thermalization sweeps from a cold start, and every 1000 sweeps thereafter.<sup>16</sup> Time slices are labeled from 1 to 24, with the  $\delta$ -function source at  $t = 4$ . A symmetric combination of the current

$$[j^\mu(x_1 - \hat{\mu}) + j^\mu(x_1)]/2$$

is centered at time slice  $t_1 = 12$ . The following calculations are done in the lab frame  $\mathbf{p} = 0$ ,  $\mathbf{p}' = \mathbf{q} = |\mathbf{q}|\hat{\mathbf{x}}$  at  $|\mathbf{q}|a = 2\pi/24$ , the minimum nonzero momentum available on our lattice. The spatial direction of the electromagnetic current is chosen in the  $z$  direction. Electric and magnetic form factors are calculated with the ratios of (2.17a) and (2.17b), respectively.

Statistical errors are calculated in a third-order, single-elimination jackknife, with bias corrections.<sup>17</sup> A third-order jackknife provides uncertainty estimates for the correlation functions, fits to the correlation functions, and quantities extrapolated to the chiral limit.

### III. RESULTS

#### A. Baryon mass and two-point functions

In the standard model, fermion masses are not calculable from first principles. Fortunately, the masses of  $u$  and  $d$  quarks are small on the scale of QCD and are not significant in present lattice calculations. We extrapolate the masses of the light  $u$  and  $d$  quarks to the chiral limit. On the other hand, the strange-quark mass is much larger, and as we shall see, plays a major role in the un-

derstanding of the electromagnetic properties of the baryon octet.

To account for the heavier mass of the strange quark we fix  $\kappa_s = \kappa_1 = 0.152$ , the smallest value of  $\kappa$  considered. We need some indication that this choice of  $\kappa_s = \kappa_1$  gives a reasonable description of the strange-quark dynamics. Figure 1 displays the masses of the octet baryons obtained from the two-point functions of  $\chi_1$ . The pion mass is extrapolated to zero to determine  $\kappa_{cr}$ . The nucleon mass is used to set the scale for the lattice results. The experimental measurements<sup>18</sup> of the hyperon masses indicate our selection of  $\kappa_s = \kappa_1$  for the strange quark gives a reasonable description of the strange-quark dynamics. The statistics of the lattice results are not sufficient to reveal the small experimental splitting of approximately 75 MeV between  $\Sigma$  and  $\Lambda$ . However, we do find the mass of  $\Sigma$  larger than  $\Lambda$  on average.

An investigation of the two-point correlation functions corresponding to the octet interpolating fields  $\chi_1$  and  $\chi_2$  in the SU(3) limit reveals that  $\chi_2$  has relatively little overlap with the ground state. By time slice 12 the overlap of  $\chi_2$  with the ground state is approximately 2 orders of magnitude less than that of  $\chi_1$ . Beyond time slice 12 the correlation functions of  $\chi_2$  become noisy. Similar results are found for larger values of  $\kappa$ . The interpolating field of  $\chi_2$  vanishes in the nonrelativistic limit and at our values of  $\kappa$  the quarks are somewhat heavier than the generally accepted masses of a few MeV. Since  $\chi_2$  has relatively little overlap with the ground state on our lattice, linear combinations of  $\chi_1 + b\chi_2$  where  $|b| \leq 1$  (typically considered in the sum-rule approach) must yield similar results. We consider the case for  $b = -1$  in the proton and present the results for inspection in the tables of the Appendix. A more important consideration is whether  $\chi_2$  yields the same results as  $\chi_1$ . The correlation function of  $\chi_2$  is too noisy to make a firm statement. However, our results do not provide any evidence to the contrary. In the following, all results are obtained from consideration of the interpolating fields of type  $\chi_1$  alone.

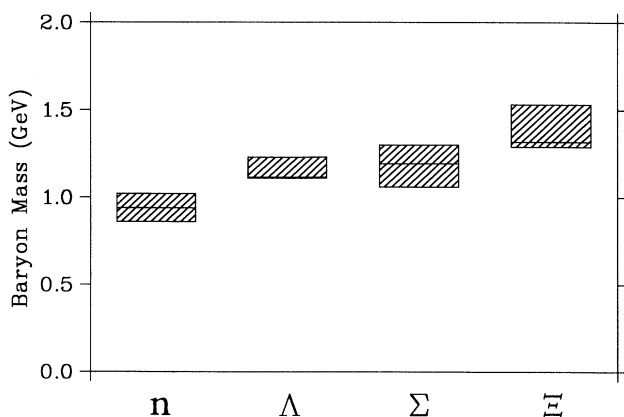


FIG. 1. Octet-baryon masses. The nucleon mass is used to set the scale for the lattice results. The experimental measurements of the hyperon masses indicate our selection of  $\kappa_s = \kappa_1 = 0.152$  for the strange quark gives a reasonable description of the strange-quark dynamics.

## B. Correlation function ratios

The ratio of (2.15) is calculated on the lattice using the correlation functions discussed in Sec. II C. Three values of  $\kappa$  for the  $u$  and  $d$  quarks with  $\kappa_s = \kappa_1$  are investigated. Figure 2 displays the ratio of (2.15) proportional to the electric form factor for  $\Sigma^+$  at  $\kappa_3 = 0.156$ . Fortunately there is a rather broad plateau away from the lattice boundary where the electric form factor may be extracted using (2.17a).

We consider fits of the correlation functions from time slice 15 through to 21 in intervals including 4 to 7 points. The results are selected from these 10 fits based on the flatness of the correlation functions and the statistical uncertainties. It is found that fits of the 5 points in the time slice interval 16 to 20 provide the optimum balance between these systematic and statistical uncertainties.<sup>19</sup> The strange-quark contributions are based on a smaller value of  $\kappa$  and therefore are less sensitive to fluctuations in the gauge fields. As a result, the error bars of the strange-quark contributions are smaller than those of the  $u$  quarks. Properties in which the strange-quark contributions dominate are generally determined with smaller statistical uncertainties.

Figure 3 illustrates the ratio of correlation functions proportional to the magnetic form factor for  $\Xi^0$ . The negative contribution of the  $u$  quark to the total magnetic moment indicates the spin projection of the  $u$  quark is opposite that of the doubly represented  $s$  quarks for the majority of time. It follows that doubly represented quarks spend most of the time paired with their spins aligned in a symmetric spin-1 state. It is interesting to note that, while the magnitude of the combined charge of the  $s$  quarks equals the  $u$ -quark charge, the heavier  $s$  quarks make a contribution to the magnetic form factor roughly double that of the  $u$  quark. Of course, this is in qualitative agreement with the predictions of SU(6) spin-flavor symmetry.

We have displayed the ratios of three-point correlation functions for only 2 of the 24 ratios considered. In the Appendix we summarize these calculations in 11 tables

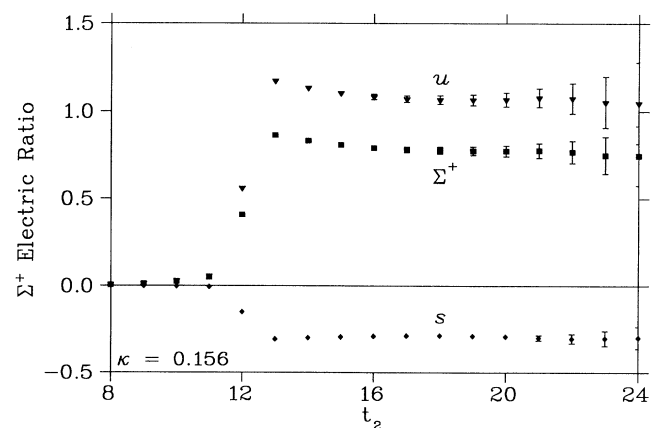


FIG. 2. Ratio of three-point correlation functions proportional to the electric form factor of  $\Sigma^+$ . The quark sector contributions are also displayed.

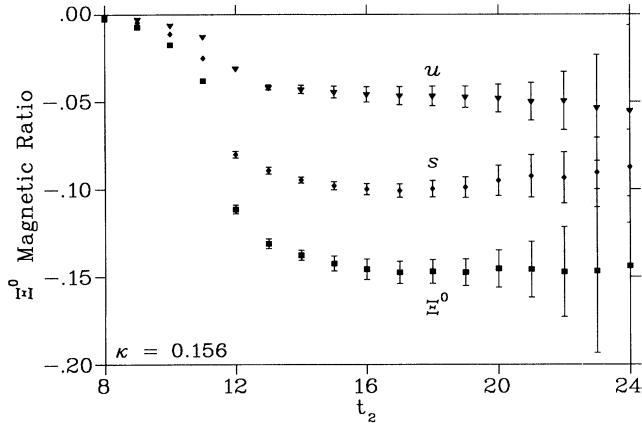


FIG. 3. Ratio of three-point correlation functions proportional to the magnetic form factor of  $\Xi^0$ .

indicating the electric and magnetic form factors calculated at the smallest finite value of  $q^2$  available on our lattice. Contributions from the different quark sectors are also illustrated. The form factors are given for the three values of  $\kappa$  considered as well as for the extrapolated results. Since  $q^2$  varies only slightly with  $\kappa$  it is reasonable to make the extrapolation to the chiral limit.

At  $\kappa = \kappa_1$ , SU(3) symmetry is exact, and the SU(3) predictions<sup>20</sup>  $p = \Sigma^+$ ,

$$n = 2\Lambda = -2\Sigma^0 = \Xi^0 = \frac{2\sqrt{3}}{3} |\Sigma^0 \rightarrow \Lambda|,$$

and  $\Sigma^- = \Xi^-$ , and the SU(2) prediction  $\Sigma^0 = (\Sigma^+ + \Sigma^-)/2$  for the electromagnetic form factors may be checked. Most of these symmetries are apparent in the correlation functions and are satisfied exactly on the lattice. For the interpolating field  $\Lambda_C$ , the relations are not exactly satisfied since the correlation function is not the full octet form. However, the SU(3) relations agree within the statistical uncertainties.

Throughout this analysis we calculate many properties for both interpolating fields  $\Lambda_C$  and  $\Lambda_8$ . In every case the results corresponding to these two interpolating fields agree within uncertainty. Calculations of splitting between the results also reveal splittings in agreement with zero. For example, the difference of the electric form factors calculated with  $\Lambda_8$  and  $\Lambda_C$  is 0.005(16). The difference of the magnetic form factor is 0.003(65). This confirms the independence of the results from the form of the interpolating field.

### C. Electric properties

The electric charge radius of a baryon may be extracted from the electric form factor with the standard small  $q^2$  expansion of the Fourier transform of a spherical charge distribution by

$$\langle r^2 \rangle = -6 \frac{d}{dq^2} \mathcal{G}_E(q^2) \Big|_{q^2=0}. \quad (3.1)$$

We have two points describing the function  $\mathcal{G}_E(q^2)$ ,

namely  $\mathcal{G}_E(0)$ , the total charge of the baryon, and  $\mathcal{G}_E(q^2)$  evaluated at the smallest finite value of  $q^2$  available on our lattice. To evaluate the derivative of (3.1) we need an analytical form for the function  $\mathcal{G}_E(q^2)$ . It is well known that the experimental electric form factor of the proton may be fit in a dipole approximation:

$$\mathcal{G}_E(q^2) = \frac{\mathcal{G}_E(0)}{(1 + q^2/m^2)^2}, \quad q^2 \geq 0. \quad (3.2)$$

We will use this form to describe the  $q^2$  dependence of the electric form factors of the charged baryons. The dipole mass  $m$  is determined by the two known values of  $\mathcal{G}_E$  yielding the dipole result

$$\frac{\langle r^2 \rangle}{\mathcal{G}_E(0)} = \frac{12}{q^2} \left[ \left( \frac{\mathcal{G}_E(0)}{\mathcal{G}_E(q^2)} \right)^{1/2} - 1 \right]. \quad (3.3)$$

To assess the sensitivity of our results on the dipole approximation we also consider the monopole form which gives

$$\frac{\langle r^2 \rangle}{\mathcal{G}_E(0)} = \frac{6}{q^2} \left[ \frac{\mathcal{G}_E(0)}{\mathcal{G}_E(q^2)} - 1 \right]. \quad (3.4)$$

In the tables of the Appendix we have quoted the quantity  $\sqrt{\langle r^2 \rangle} / \mathcal{G}_E(0)$ , which gives the radius of baryons and quark distributions with unit charge. In all cases the sign of  $\langle r^2 \rangle$  is the same as the charge of the baryon or quark. The difference of the radii extracted in the dipole and monopole approximations is small relative to the statistical uncertainties in the radii. We refer to the dipole results in the following discussion and figures.

Of the four charged baryons only the charge radius of the proton has been experimentally measured. The lattice spacing  $a$  may be determined using the experimental nucleon mass  $M_N$ , setting  $M_N a = 0.61(5)$ . This yields  $a = 0.128(11)$  fm. Hence the lattice prediction of the proton radius is 0.65(8) fm, which is somewhat smaller than the experimental measurement<sup>21</sup> of 0.862(12) fm. It is interesting to note that the lattice proton radius is roughly the same as that for the pion.<sup>7</sup>

Finite lattice size effects may be the cause of the discrepancy between the lattice and experimental radii. At  $\kappa = \kappa_3$  the proton diameter is approximately 9 lattice units (LU) and therefore largely fills the lattice in the  $y$  and  $z$  directions which are 12 LU in length. Since we have used periodic boundary conditions in the spatial directions, our baryon under study is actually surrounded by six identical baryons. Overlap of the wave functions may cause the size of the baryon to be reduced.

Figure 4 displays the lattice predictions of the electric charge radii for the charged members of the baryon octet. We have included the results of two recent model calculations for comparison with the lattice results. The quark model<sup>22</sup> and Skyrme model<sup>23</sup> results have been scaled to agree with the lattice proton result and are indicated by the dashed lines in Fig. 4. The same pattern of relative sizes of the baryons is observed in each calculation. The only significant difference is the rather small Skyrme model radius for  $\Xi^-$ .

It should be noted that although the uncertainty re-

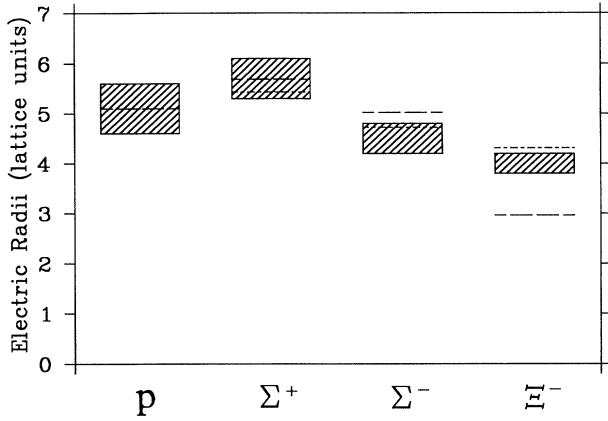


FIG. 4. Electric charge radii of the charged octet baryons. The short-dashed lines correspond to the quark-model results<sup>22</sup> and the long-dashed lines correspond to the Skyrme-model results.<sup>23</sup> The model results are scaled to the proton lattice radius.

gions of the radii for different baryons overlap it does not necessarily mean that the proton, for example, may be larger than  $\Sigma^+$ . The uncertainties are highly correlated between the two results and a calculation of the difference of the radii indicates  $\Sigma^+$  is larger by  $0.60^{+0.35}_{-0.15}$  LU. Similar results hold for the other baryons.

To gain some understanding of this pattern we must look at the underlying dynamics of the quarks in the baryons. By coupling the electromagnetic field to only  $u$  quarks, for example, we can examine the role of the  $u$  quark and how it differs within various baryons. There are two effects that cause the charge radius of  $\Sigma^+$  to be larger than that of the proton. Figure 5 displays the radii of  $u$ - and  $s$ -quark distributions within  $\Sigma^+$  as the  $u$  quarks are extrapolated to  $\kappa_{cr}$ . The radius of the  $u$  quark distribution increases as the  $u$  quark becomes lighter (smaller  $\kappa^{-1}$ ), as expected. However, note that the radius of the  $s$ -quark distribution decreases as the  $u$  quarks become lighter. A calculation of the change in the  $s$ -quark distribution radius confirms that the radius is strictly decreasing. Recall that the strange quark was fixed at  $\kappa_s = \kappa_1$ . This effect is due to the shifting of the center of mass of the  $u$ - $s$  system towards the strange quark which becomes relatively heavier as the  $u$  quarks become lighter. With the center of mass closer to the  $s$  quark, the  $u$  quarks are pushed out to larger radii than in the proton. Of course there is a reduced mass effect that reduces the average distance between the  $u$  and  $s$  quarks in  $\Sigma^+$  relative to  $u$  and  $d$  quarks in  $p$ . Therefore, the overall effect is not large. A calculation of the  $u$ -quark radius difference between  $\Sigma^+$  and  $p$  indicates the  $u$ -quark distribution is larger in  $\Sigma^+$  by  $0.20^{+0.45}_{-0.15}$  LU. A similar but more pronounced effect may be seen by comparing the  $u$  quark distribution in  $n$  and in  $\Xi^0$ . Here the two  $d$  quarks in  $n$  are replaced by two  $s$  quarks in  $\Xi^0$ . The center of mass is shifted towards the strange quarks in the  $\Xi^0$  system and causes the  $u$ -quark radius to be increased by  $0.50^{+0.65}_{-0.15}$  LU over the  $u$ -quark radius in  $n$ . The effect is roughly double that in the  $p$ - $\Sigma^+$  case as one might expect.

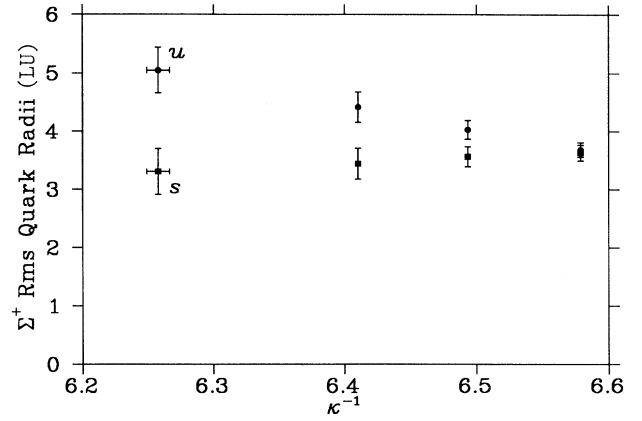


FIG. 5. Extrapolation of the electric charge distributions of quarks within  $\Sigma^+$ . While  $\kappa_s$  is fixed, the radius of the  $s$ -quark distribution is seen to decrease in the extrapolation.

The main dynamics causing  $\Sigma^+$  to appear larger is the reduced  $s$ -quark contributions in the charge radius relative to the  $d$  quark in the proton. Since the  $d$  quark is lighter, its distribution is broader at 4.4(8) LU in the proton compared to 3.3(4) LU for the  $s$  quark in  $\Sigma^+$ . Hence the  $d$  quark makes a larger reduction of the  $u$ -quark contributions in the proton charge radius than the  $s$  quark in  $\Sigma^+$ .

$\Sigma^-$  appears smaller than  $\Sigma^+$  since the total charge at large radius (the two  $d$ -quarks) is half that in  $\Sigma^+$ . However, the  $s$  quark acts to increase the charge radius in  $\Sigma^-$  increasing the charge radius to well over half that of  $\Sigma^+$ . Similarly  $\Xi^-$  appears smaller than  $\Sigma^-$  since one of the  $d$  quarks at large radius in  $\Sigma^-$  has been replaced by an  $s$  quark at smaller radius, reducing the total charge radius.

It is well known that the charge radius of the neutron is particularly sensitive to the curvature of the form factor at  $q^2=0$ . At our value of  $q^2 \simeq 4 \text{ fm}^{-2}$  we do not have the information necessary to reliably determine the electric charge radius. However, through the relation of (3.1), it is fair to assume some scaling of the electric form factor and the corresponding charge radius. Figure 6 displays the electric form factors, of the neutral members of the baryon octet. The lattice results suggest a negative value for the squared charge radius in the neutron, and positive squared charge radii for the hyperons.

The negative squared charge radius of the neutron indicates the two  $d$  quarks have a larger charge radius than the  $u$  quark within the neutron. A calculation of the  $d-u$  quark radius difference indicates the  $d$ -quark distribution is larger by  $0.45^{+0.70}_{-0.40}$  LU. These results are in agreement with a quark model<sup>24</sup> where the spin-dependent interaction splitting the nucleon and  $\Delta$  states is more repulsive for the doubly represented  $d$  quarks, which are more likely to be in a spin-1 state than are the  $u$ - $d$  pairs.

The total charge of the light quarks in  $\Lambda$  and  $\Sigma^0$  is  $+\frac{1}{3}$  and makes a larger contribution to the charge radii than the oppositely charged more massive  $s$  quarks. Hence, the squared charge radius is positive and the electric

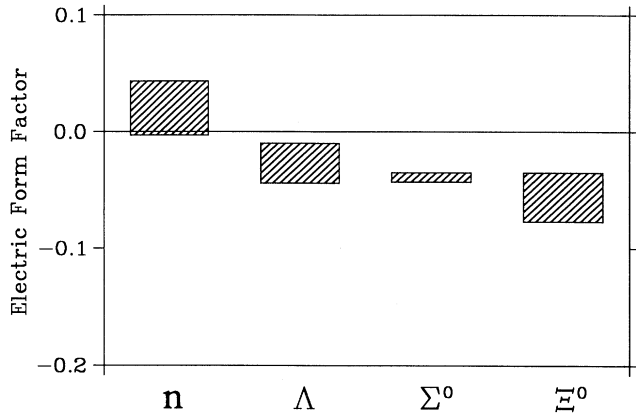


FIG. 6 Electric form factors of the neutral charge baryons. The lattice results suggest a negative charge radius for the neutron, and positive charge radii for the hyperons.

form factor at our value of  $q^2$  is negative.

The electric form factor of  $\Xi^0$  is interesting since the repulsive spin effect acts between the two  $s$  quarks. However this effect is small compared to the mass effects of the  $u$ - $s$ -quark system. Here the total charge of the light  $u$  quark is  $+\frac{2}{3}$  and makes a larger contribution to the charge radius than the oppositely charged  $s$  quarks at smaller radii. Hence, the squared charge radius is positive and the electric form factor at our value of  $q^2$  is negative. Furthermore the charges involved are double that in the case of  $\Lambda$  or  $\Sigma^0$ . Correspondingly the electric form factor is roughly double that of  $\Lambda$  or  $\Sigma^0$ . Figure 7 shows the distributions of the  $u$  and  $s$  quarks within  $\Xi^0$  as the  $u$  quarks are extrapolated to  $\kappa_{cr}$ . Note that at  $\kappa=\kappa_1$ , the SU(3)-flavor-symmetry limit, the two  $s$  quarks have a larger radius than the  $u$  quark, similar to the  $d$  quarks in the neutron. However, away from the SU(3) limit, the mass effects are seen to dominate quickly.

#### D. Magnetic moments

Our calculation of magnetic form factors is done at the smallest finite value of  $q^2$  available on our lattice. On the other hand, the magnetic moment is defined at  $q^2=0$  as  $\mu/(e/2M_B)=\mathcal{G}_M(0)$  and therefore we must scale our results from  $\mathcal{G}_M(q^2)$  to  $\mathcal{G}_M(0)$ . Note that  $\mathcal{G}_M(0)$  gives the magnetic moment  $\mu$  in units of natural magnetons  $\mu_B=e/2M_B$  where the mass of the baryon  $M_B$  appears in the definition of the magneton. Lattice extrapolations in  $q^2$  to  $q^2=0$  suffer from large statistical errors. To make contact with the experimental magnetic moments, we assume a scaling of electric and magnetic form factors in  $q^2$ . This is suggested by the experimentally measured relation

$$\frac{\mathcal{G}_M(q^2)}{\mathcal{G}_M(0)} \simeq \frac{\mathcal{G}_E(q^2)}{\mathcal{G}_E(0)}, \quad (3.5)$$

for proton form factors. For the neutral members of the baryon octet, the procedure is not as clear. The magnetic form factor of  $n$  scales as the electric form factor of  $p$  al-

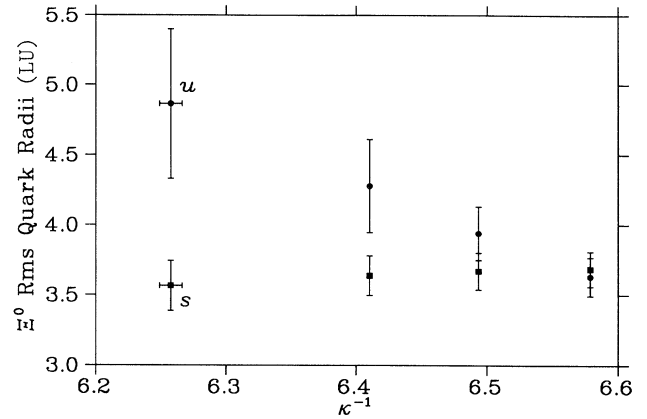


FIG. 7. Extrapolation of the electric charge distributions of quarks within  $\Xi^0$ . The mass effect of the strange quark is seen to dominate quickly in the radii of the quark distributions.

lowing a calculation of the neutron magnetic moment. However, the electric form factors of  $\Sigma^+$  and  $\Sigma^-$  are different and therefore it is not clear how to scale the results for  $\Sigma^0$  to  $q^2=0$ .

The solution lies in the understanding of the differences in the electric form factors of  $\Sigma^+$  and  $\Sigma^-$ . We have seen that there are two effects which govern the electric properties. In cases of equal-mass quarks we have seen evidence of a spin-dependent force which acts differently on the doubly represented quarks. However when the strange quark is involved the effects are dominated by the heavier strange-quark mass. These differing sectors do not scale in the same manner and therefore (3.5) may not be appropriate for hyperons. Instead we use (3.5) to scale the individual quark sectors to  $q^2=0$ . For example, the strange-quark contributions are scaled by

$$\frac{\mathcal{G}_M^s(q^2)}{\mathcal{G}_M^s(0)} = \frac{\mathcal{G}_E^s(q^2)}{\mathcal{G}_E^s(0)}, \quad (3.6)$$

and similarly for the light quarks, such that the magnetic moment of a hyperon is given by

$$\mathcal{G}_M^B(0) = \mathcal{G}_M^l(0) + \mathcal{G}_M^s(0), \quad (3.7)$$

where  $l$  labels the light quarks. Similarly, in  $p$  and  $n$  the  $u$  and  $d$  sectors are scaled separately. In the  $\Sigma^0 \rightarrow \Lambda$  transition moment, the strange quark does not contribute. In this case the electric properties of the light quarks in  $\Sigma^0$  are used to scale the transition moment to  $q^2=0$ . The tables of the Appendix list the magnetic moments of the baryons as well as the quark sector contributions in units of natural magnetons  $\mu_B$ . In the proton for example,  $\mathcal{G}_M^u(0)$  gives the combined magnetic moment contributions of both  $u$  quarks. Note that the magnetic moment of  $\Lambda$  is largely determined by the  $s$ -quark contributions as in the simple quark model.

With the magnetic moments of the baryons completely defined, we may now consider the SU(6) predictions for the ratios of magnetic moments. We have selected the ratios  $n/p$ ,  $\Sigma^-/\Sigma^+$ , and  $\Xi^-/\Xi^0$ . These ratios, in conjunc-

tion with the SU(3) relations, allow a calculation of all the SU(6) ratios. The results are summarized in Table I. While there is qualitative agreement with the SU(6) predictions, the lattice results indicate some deviation in the hyperon ratios.

To gain a deeper understanding of these deviations, it is useful to consider the individual quark sector contributions to the magnetic moments. In the simple quark model, the magnetic moment of the proton is given by

$$\mu^p = \frac{4}{3}\mu^u - \frac{1}{3}\mu^d. \quad (3.8)$$

In the SU(2) limit where  $\mu^u = -2\mu^d$ , the ratio of the quark sector contributions in the simple quark model is  $\frac{4}{3}\mu^u / -\frac{1}{3}\mu^d = 8$ . The lattice results differ significantly from this prediction of SU(6) spin-flavor symmetry. At  $\kappa_1$  this ratio of quark sector contributions is 10.3(7). The fact that the ratio is larger indicates an enhancement of the doubly represented  $u$ -quark contributions relative to the  $d$  quark. Similar results hold for the other baryons of the octet. Although the lattice results reproduce the SU(6) ratios for hadrons considered in Table I reasonably well, the ratio of different quark sector contributions shows the underlying quark dynamics are really quite different.<sup>25</sup>

The same effect may be seen by comparing the effective moment of the  $u$  quark in the proton with the effective moment of the  $u$  quark in the neutron. We define the effective moment of the lattice  $u$  quark in the proton by equating the lattice  $u$ -quark sector contribution to  $\frac{4}{3}\mu^u$ , the corresponding  $u$ -quark sector contribution in the simple quark model. Similarly, in the neutron the lattice  $u$ -quark contribution is equated with  $-\frac{1}{3}\mu^u$ . One can define effective moments for quarks in other baryons in a similar manner. In the proton we find  $\mu^u = 1.48(8) \mu_N$ , while in the neutron  $\mu^u = 1.14(9) \mu_N$ , at  $\kappa_1$ , the SU(3) limit. A careful examination of the simple-quark-model ratios of magnetic moments indicates this effect is responsible for the lattice deviations from SU(6) symmetry indicated in Table I.

Away from the SU(3)-flavor limit, one can search for quark mass effects analogous to those seen in the electric properties. Of course, the effective moment of the strange quark is smaller than the light quarks as expected. However, there are more subtle effects seen in the effective magnetic moments of the quarks which are due to the shifting of the center of mass. For example, consider the  $u$ -quark contribution to the magnetic moments of  $n$  and  $\Xi^0$ . In the SU(3)-flavor limit, the effective moments of the  $u$  quark in these two baryons are found to be

TABLE I. Magnetic-moment ratios in SU(3)-flavor symmetry.

Ratio	SU(6) symmetry	Lattice results
$n/p$	$-\frac{2}{3}$	$-0.63(5)$
$\Sigma^-/\Sigma^+$	$-\frac{1}{3}$	$-0.37(3)$
$\Xi^-/\Xi^0$	$\frac{1}{2}$	$0.58(5)$

the same. However, with the light quarks extrapolated to  $\kappa_{cr}$  we find the  $u$ -quark contribution to the neutron magnetic moment is  $-0.25(17) \mu_N$ , while the  $u$ -quark contribution in  $\Xi^0$  is larger at  $-0.36(5) \mu_N$ . This effect, due to unequal quark masses, is not accounted for in a constituent quark picture.

Figure 8 displays the lattice predictions of magnetic moments in units of natural magnetons. Experimental moments<sup>18</sup> are shown in solid black. The magnetic moments of the baryons in nuclear magnetons  $\mu_N$  are indicated in Table II along with ratios of the proton magnetic moment. While the signs of the moments are correctly determined, the moments appear to be underestimated by an amount that appears to be constant in magnitude for most baryons. The only notable exception is that of  $\Lambda$ .

It is difficult to determine the origin of this discrepancy. At our value of  $\beta=5.9$  there may be some deviations from asymptotic scaling. Nonquenched corrections may provide additional contributions. However, there are other interesting candidates. One possible factor in the discrepancy is the contribution of disconnected quark loops to the magnetic moments. We have not included the case where a photon interacts with a quark loop in the vacuum which in turn interacts via gluons with the valence quarks of the baryons.

These loop contributions are expected to be similar for the proton and neutron and therefore cannot provide the complete solution. However, the importance of the loop effects may be estimated by comparing the predictions of the isoscalar magnetic moment with the isovector magnetic moment. On the lattice we have enforced isospin symmetry by equating  $\kappa_u = \kappa_d$  and therefore loop effects do not contribute to the isovector magnetic moment. The lattice/experimental ratio of magnetic moments in the isoscalar channel is 1.1(3), while in the isovector channel we find 0.8(2). Hence loop corrections may improve the agreement in the isoscalar channel; however, there may be larger unaccounted corrections in the isovector channel.

Perhaps the most compelling candidate causing the un-

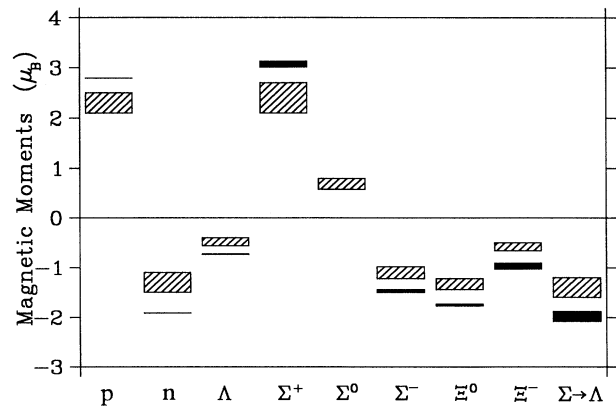


FIG. 8. Magnetic moments of the baryon octet in natural magnetons. Experimental moments and uncertainties are indicated in solid black. While the signs of all moments are correctly determined, the magnitudes of the moments are underestimated.

TABLE II. Magnetic moments in nuclear magnetons ( $\mu_N$ ).

Baryon	Lattice results		Experimental measurements (Ref. 18)	
	( $\mu_N$ )	$\mu/\mu_p$	( $\mu_N$ )	$\mu/\mu_p$
$p$	2.3(3)	1	2.793	1
$n$	-1.3(2)	-0.57(8)	-1.913	-0.685
$\Lambda$	-0.40(7)	-0.18(3)	-0.613(4)	-0.219(2)
$\Sigma^+$	1.9(2)	0.85(6)	2.42(5)	0.866(18)
$\Sigma^0$	0.54(9)	0.23(2)		
$\Sigma^-$	-0.87(9)	-0.38(4)	-1.157(25)	-0.414(9)
$\Xi^0$	-0.95(8)	-0.42(4)	-1.250(14)	-0.448(5)
$\Xi^-$	-0.41(6)	-0.18(2)	-0.69(4)	-0.25(2)
$\Sigma \rightarrow \Lambda$	-1.15(16)	-0.51(8)	-1.61(8)	-0.58(3)

derestimation of the magnetic moments is finite-volume effects. In the discussion of electric charge radii we argued that overlap of the surrounding baryons may cause the size of the baryon under study to be restricted. In a similar fashion, the magnitude of the magnetic moments may be reduced. Such an effect also accounts for the smaller discrepancy in the magnetic moment of  $\Lambda$ . Here the origin of the magnetic moment is largely from the  $s$  quark. Strange quark distributions are more localized and therefore finite-volume effects are expected to be less important.

In Table II we have also included the ratios of the magnetic moments with the proton magnetic moment. This allows a more detailed comparison with the experimental measurements. Most ratios agree with the experimental ratios at the  $1\sigma$  level; however, all the lattice ratios are small in magnitude. Only the ratios of  $n$  and  $\Xi^-$  fail to agree at the  $1\sigma$  level. The underestimation of the magnitude of the ratios is most likely due to the underestimation of the magnetic moments themselves. Adding a constant amount to the magnitudes of the numerator and denominator of the ratios acts to increase the magnitude of the ratios.

### E. Magnetic radii

Magnetic radii may be determined in exactly the same fashion as that for electric radii indicated in (3.3) and (3.4). The lattice prediction of the proton magnetic radius of 0.60(9) fm is small compared to the experimental measurement<sup>21</sup> of 0.858(56) fm. Similarly the lattice prediction of the neutron magnetic radius of 0.58(9) fm is small compared to the experimental measurement of 0.876(70) fm. The lattice results suggest the magnetic radius of the proton may be larger than that of the neutron by  $0.02^{+0.08}_{-0.01}$  fm and smaller than the electric radius of the proton by 0.05(5) fm. Unfortunately, the uncertainties in the experimental results are too large to make a statement on these estimates.

In Fig. 9 we have plotted  $\sqrt{|\langle r^2 \rangle / \mathcal{G}_M(0)|}$  for each baryon of the octet. Both lattice and Skyrme model results are shown. All values of  $\langle r^2 \rangle / \mathcal{G}_M(0)$  are positive in the lattice results; however,  $\langle r^2 \rangle / \mathcal{G}_M(0)$  for  $\Xi^-$  is negative in the Skyrme model. Generally speaking the two calculations reproduce the same pattern of magnetic radii

with the exception of  $\Xi^-$ .

The small magnetic radius of  $\Lambda$  is consistent with the fact that the strange quark dominates in the quark contributions to the magnetic moment. The magnetic radius of  $\Sigma^-$  is interesting since it is the largest of the octet baryons including  $\Sigma^+$ , which has the largest electric charge radius. The magnetic radius is larger for  $\Sigma^-$  due to cancellation between the  $d$ - and  $s$ -quark contributions to the magnetic moment. In  $\Sigma^-$  the  $s$  quark acts to decrease the magnitude of the magnetic moment. As the resolution of the interaction increases, information on the broadly distributed  $d$  quarks is lost at a faster rate than the  $s$  quark. This results in a large decrease in the magnitude of the total magnetic moment and corresponds to a large magnetic radius.

The magnetic properties of  $\Xi^-$  are particularly interesting. Of the octet baryons,  $\Xi^-$  is really the only candidate for a negative magnetic radius  $\langle r^2 \rangle / \mathcal{G}_M(0)$ . To have  $\langle r^2 \rangle / \mathcal{G}_M(0) < 0$  requires  $|\mathcal{G}_M(0)| < |\mathcal{G}_M(q^2)|$  as indicated in (3.3) and (3.4). That is, as the resolution of the interaction is increased, the magnitude of the magnetic form factor increases. Hence we require a baryon in

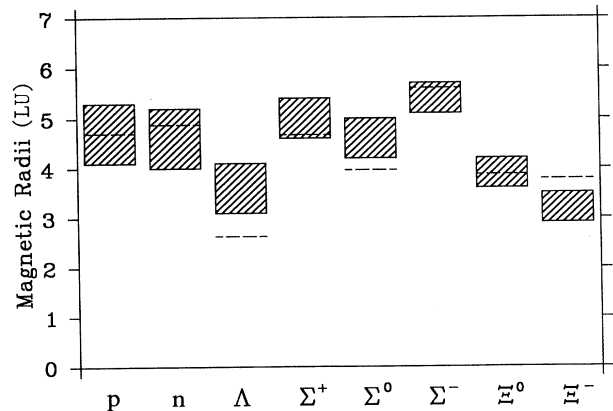


FIG. 9. Magnetic radii of the baryon octet. Dashed lines indicate Skyrme model results which are scaled to agree with the proton magnetic lattice radius. The pattern of the radii appear quite similar in the two calculations. All values of  $\langle r^2 \rangle / \mathcal{G}_M(0)$  are positive in the lattice results, however,  $\langle r^2 \rangle / \mathcal{G}_M(0)$  for  $\Xi^-$  is negative in the Skyrme model.

which the contributions of a relatively light quark act to decrease the magnitude of the baryon magnetic moment. In  $\Lambda$  the light quarks do not make sufficient contributions to have any significant effect on the magnetic radius. The two  $s$  quarks of  $\Xi^-$  contribute a magnetic moment of  $-0.83(7) \mu_B$  while the  $d$  quark acts to reduce the magnetic moment by  $0.25(4) \mu_B$  to the lattice prediction of  $-0.58(8) \mu_B$ . It is possible that as the resolution of the interaction increases, the reducing influence of the  $d$  quark is lost at a sufficient rate relative to the  $s$  quark, such that the magnitude of the magnetic moment increases. However, this is not the case in the lattice results. In any event, the magnetic properties of  $\Xi^-$  are a sensitive probe of the relative dynamics of  $s$  and  $d$  quarks.

To further examine the roles of the light and heavy quarks we have taken the ratio of  $\Xi$  and  $\Lambda$  magnetic moments. In the simple quark model the magnetic moment ratio for  $\Xi^-$  and  $\Lambda$  is

$$\frac{\mu_{\Xi^-}}{\mu_{\Lambda}} = \frac{1}{3} \left[ 4 - \frac{\mu^d}{\mu^s} \right] \quad (3.9)$$

and similarly for  $\Xi^0$  with  $d \rightarrow u$ . Clearly this ratio reflects the relative roles of strange and light quarks. If the contribution of the  $d$  quark ( $u$  quark) is overestimated relative to the  $s$  quark then the magnetic moment of  $\Xi^-$  ( $\Xi^0$ ) is underestimated (overestimated) and the magnetic radius of  $\Xi^-$  may appear negative.

Table III displays these ratios for a number of different calculations. Note that the simple quark model ratio of (3.9) cannot reproduce the experimental ratio of  $\Xi^-/\Lambda$  with a strange quark heavier than the  $d$  quark. The simple quark model fails because the intrinsic magnetic moments of the constituent quarks are not dependent upon spin dynamics or the baryon in which the quarks reside. Consider, for example, the ratio of the  $s$ -quark sector contributions to the magnetic moments of  $\Xi^-$  and  $\Lambda$ . Equation (3.9) indicates this ratio is  $4/3$  in the simple-quark model. In contrast, the ratio of the  $s$ -quark contributions is  $1.6(2)$  on the lattice. This leads to closer agreement between the lattice and experimental  $\Xi^-/\Lambda$  magnetic moment ratio.

The sum-rule results<sup>26</sup> are particularly poor for the  $\Xi^-/\Lambda$  ratio. In the sum-rule approach it is possible to estimate the importance of excited-state approximations, nonperturbative contributions, and strange-quark-mass effects. This is done by comparing the sum-rule prediction of the magnetic moment with a zeroth-order calculation where only the leading order perturbative contributions of massless quarks are included in the operator-product expansion. Similarly, contributions of excited state baryons are not included at the hadronic level. Of

the octet baryons,  $\Xi^-$  has the largest correction to the zeroth-order result.

Although the Skyrme model is restricted to mesonic degrees of freedom, it bears a behavior very similar to the discussion of (3.9). The fact that the lattice results reproduce the experimental ratio for  $\Xi^-/\Lambda$  better than the Skyrme model lends credence to our prediction of a positive value of  $\langle r^2 \rangle / \mathcal{G}_M(0)$  for  $\Xi^-$ .

## F. Magnetic moment ratios

Explaining the magnetic moments of baryons has been a long-standing problem of hadronic physics. In Fig. 10 we have collected together recent results of the best-known approaches to QCD. We have included the results of SU(6) symmetry, the QCD sum-rule (SR) approach,<sup>26</sup> lattice (Latt.) calculations, quark-model (QM) results<sup>2</sup> and Skyrme (Skyr.) model results<sup>23</sup>. Note that the experimental result, and sum-rule result for  $\Sigma^0$  is obtained using the SU(2) relationship  $\mu_{\Sigma^0} = (\mu_{\Sigma^+} + \mu_{\Sigma^-})/2$ .

Four parameters in the quark model<sup>22</sup> were determined with reference to hadronic ground-state masses. These quark-model results are very similar to those of the simplest quark model<sup>18</sup> where the  $p$ ,  $n$ , and  $\Lambda$  magnetic moments are used as inputs to determine the intrinsic quark moments. The quark model does not reproduce the magnetic moment ratios as well as the lattice or sum-rule results.

Two parameters in the Skyrme model<sup>23</sup> are determined with the  $n$  and  $\Delta$  masses. The Skyrme model reverses the order of many of the SU(6) partners including  $p$  and  $\Sigma^+$ ,  $\Lambda$  and  $\Xi^-$ , as well as  $\Xi^0$  and  $n$ .

Vacuum susceptibility parameters in the sum-rule approach<sup>26</sup> are optimized to give the best agreement with the experimental magnetic moments. The sum-rule and lattice results appear very similar with the exception of  $\Xi^-$  where the correction to the zeroth-order sum-rule estimate is largest in the sum-rule approach.

Once the quark masses are fixed, our calculation of the magnetic moments is parameter-free. With the exception of the neutron, the lattice results are a significant improvement over the SU(6) symmetry ratios and predict the experimental ratios reasonably well. The lattice results outperform the model calculations in reproducing the experimental magnetic moment ratios. As previously discussed the discrepancies in the neutron lattice results may be due to finite-volume effects.

TABLE III.  $\Xi/\Lambda$  magnetic moment ratios.

Baryon	SU(6) symmetry	Sum rules (Ref. 26)	Lattice results	Quark model (Ref. 22)	Skyrme model (Ref. 23)	Experimental measurements (Ref. 18)
$\Xi^0/\Lambda$	2.0	2.64	2.4(5)	2.32	2.40	2.04(3)
$\Xi^-/\Lambda$	1.0	1.86	1.0(2)	0.87	0.676	1.13(7)

### G. Flavor-singlet interpolating field

The results from the flavor-singlet interpolating field are interesting only in the SU(3) limit of  $\kappa_1$ . If SU(3) symmetry is broken then one must expect some mixing of the ground state  $\Lambda$  in the correlation functions. Unfortunately, the correlation functions of the singlet interpolating field suffer from large statistical uncertainties, and therefore it is not possible to subtract the contributions of the ground state in a reliable manner.

In many cases the uncertainties in the SU(3) limit are too large to discern any difference in the results from those of the other  $\Lambda$  interpolating fields. However a few differences are clear. In a flavor singlet system, the electromagnetic moments vanish. Furthermore, although the electric properties of the quarks are similar, the magnetic properties appear quite different from those of  $\Lambda_8$  or  $\Lambda_C$ . Further details may be found in the tables of the Appendix.

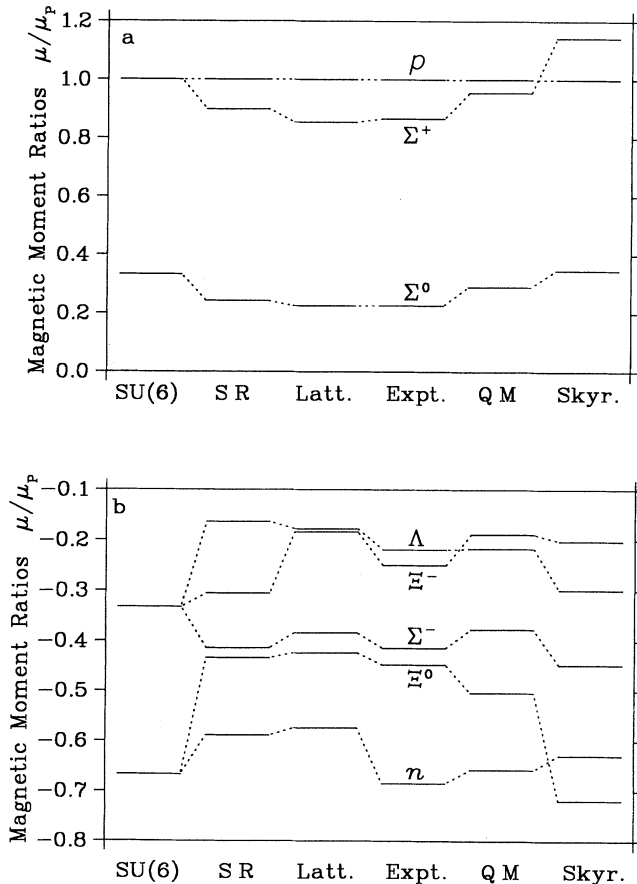


FIG. 10. A comparison of positive (a) and negative (b) magnetic moment ratio calculations. The SU(6) symmetry, QCD sum rule<sup>26</sup> (SR), lattice (Latt.), quark model<sup>22</sup> (QM) and Skyrme (Skyr.) model<sup>23</sup> calculations are compared with experimental measurements<sup>18</sup> (Expt.). The experimental result and sum-rule result for  $\Sigma^0$  is obtained using the SU(2) relationship  $\mu_{\Sigma^0} = (\mu_{\Sigma^+} + \mu_{\Sigma^-})/2$ . Uncertainties in the experimental and lattice results are indicated in Table II.

### IV. SUMMARY

We have investigated the electromagnetic properties of the baryon octet in a numerical simulation of quenched QCD on a  $24 \times 12 \times 12 \times 24$  lattice at  $\beta=5.9$ . The electric and magnetic form factors were calculated at the smallest finite value of  $q^2$  available on our lattice. From these form factors, magnetic moments, electric radii, magnetic radii, and magnetic transition moments were extracted.

The lattice results suggest there are three effects responsible for the details of the distribution of electric charge within baryons. In the case of equal mass quarks the important effect may be described as a spin-dependent force that acts repulsively between doubly represented quarks. These quarks have larger electric charge distributions, which results in a negative squared charge radius for the neutron. The electric properties of baryons involving strange quarks are altered in two ways. The dominant effect is the standard reduction of the charge radius due to the relatively large mass of the strange quark. However there is a more interesting and subtle effect. As the  $u$ - and  $d$ -quark masses become lighter the electric charge radius of the strange-quark distribution is seen to decrease indicating a shifting of the center of mass towards the strange quark. As a result, the electric radius of the light-quark distribution is increased.

The qualitative structure of the baryon magnetic moment predictions of SU(6) spin-flavor symmetry is reproduced on the lattice. However closer inspection of the lattice results shows that the way in which the different quark sectors make up the baryon magnetic moments is not as simple as in a constituent quark-model picture. The different quark sector magnetic moment contributions cannot be reproduced in a constituent quark model where the intrinsic moments of the quarks are independent of spin dynamics and center-of-mass effects. In contrast, the lattice-effective quark magnetic moments show a mass and spin dependence which reflects elements such as relativistic motion and gluon dynamics not contained in the simple quark-model picture.

The pattern of electromagnetic radii in the lattice results is seen to be generally reproduced in the model calculations that are considered. The only exception is that of  $\Xi^-$  which proves to be a sensitive probe of the quark dynamics. In  $\Xi^-$  the light  $d$  quark makes a contribution to the magnetic properties opposite that of the relatively heavy strange quarks. The  $d$ -quark contribution is enhanced by the shift in the center-of-mass towards the two strange quarks. Hence the magnetic moment and magnetic radius of  $\Xi^-$  is unusually sensitive to the balance of the light and strange sectors of the theory. The lattice results predict a positive magnetic radius  $\langle r^2 \rangle / \rho_M(0) > 0$  for  $\Xi^-$  which contrasts the Skyrme model prediction.

Calculations of baryon radii and magnetic moments underestimate the magnitude of the experimental measurements. Ratios of the magnetic moments are calculated to allow a more detailed comparison with the experimental measurements. Our results are put into perspective by including the results of quark and Skyrme-model

calculations as well as QCD sum-rule calculations. The lattice calculations outperform the model calculations in reproducing the experimental ratios.

Baryon interpolating fields vanishing in the nonrelativistic limit have little overlap with ground-state baryons on our lattice. The correlation functions corresponding to these interpolating fields are reduced by approximately 2 orders of magnitude relative to the standard interpolating fields used in lattice calculations. In most cases inclusion of this interpolating field with the standard lattice interpolating field in the analysis acts to increase the noise in the correlation functions as illustrated in Table XIV of the Appendix.

Calculations of the electromagnetic properties of hadrons may ultimately provide one of the best quantitative tests of QCD. As a result, it is important to assess the magnitude of vacuum quark loop contributions. Furthermore, there is some indication that the present volume of the lattice restricts the radii and magnetic moments of the baryons. Increasing the lattice volume should be a focus of future calculations. With the approach of extracting the electromagnetic properties of hadrons from lattice QCD firmly established, a study of the electromagnetic structure of other hadrons may be interesting. A method for extracting the four electromagnetic form factors of the spin- $\frac{3}{2}$  system on the lattice has been established.<sup>27</sup> With recent attempts to measure the  $\Omega^-$  magnetic moment,<sup>28</sup> a lattice investigation of the electromagnetic properties of the low-lying spin- $\frac{3}{2}$  baryons seems very timely, and such an analysis is currently in progress.

#### ACKNOWLEDGMENTS

The computing resources for this study were provided by the Computing Science Department and the Center

for Computational Sciences at the University of Kentucky on their IBM 3090-300E supercomputer. We thank Keh-Fei Liu for his assistance in making computing arrangements. This work was supported in part by the Natural Sciences and Engineering Research Council of Canada and the U.S. Department of Energy under Grant No. DE-FG05-84ER40154.

#### APPENDIX

Throughout our discussion we have highlighted specific examples to illustrate the manner in which the lattice QCD dynamics manifest themselves in the electromagnetic properties of baryons. Of course these features are seen throughout the baryons of the octet. To allow the reader to pursue further investigation of these properties we have collected together the results of the lattice calculations in the following tables, numbered IV through XIV. We include calculations of the mass and momentum transfer in terms of the lattice spacing  $a$ . Electric and magnetic form factors at finite-momentum transfer, and the magnetic form factor at  $q^2=0$  in natural magnetons ( $\mu_B$ ) are given for the baryon under investigation and for the quark sectors composing the baryon.

Normalized electric and magnetic radii  $\sqrt{\langle r^2 \rangle} / \mathcal{G}(0)$  of the baryon and normalized electric radii of the quark distributions in lattice units are quoted for both dipole and monopole approximations. These quantities are given for each of the three values of  $\kappa$  considered as well as the extrapolation to the chiral limit at  $\kappa_{cr}$ . Statistical uncertainties in the last digits are indicated in parentheses.

TABLE IV. Proton electromagnetic form factors and radii.

	$\kappa_1=0.152$	$\kappa_2=0.154$	$\kappa_3=0.156$	$\kappa_{cr}=0.159\ 8(2)$
Mass $a$	1.09(3)	0.96(3)	0.84(3)	0.61(5)
$q^2 a^2$	0.067 58(6)	0.067 31(7)	0.066 95(10)	0.066 1(11)
$G_E(q^2)$	0.862(8)	0.839(12)	0.82(3)	0.78(4)
$G_M(q^2)$	1.86(11)	1.83(15)	1.83(18)	1.8(2)
$G_M(0)$	2.16(12)	2.17(16)	2.22(19)	2.3(2)
$G_E^d(q^2)$	-0.289(3)	-0.284(5)	-0.281(15)	-0.27(2)
$G_M^d(q^2)$	0.165(12)	0.15(2)	0.12(5)	0.10(7)
$G_M^d(0)$	0.191(13)	0.18(2)	0.15(7)	0.12(8)
$G_E^u(q^2)$	1.151(11)	1.12(2)	1.10(4)	1.04(6)
$G_M^u(q^2)$	1.70(10)	1.68(14)	1.70(16)	1.7(2)
$G_M^u(0)$	1.97(11)	2.00(15)	2.07(16)	2.1(2)
$r_E$ dipole	3.70(13)	4.04(18)	4.4(3)	5.1(5)
$r_M$ dipole	3.71(13)	3.99(17)	4.2(4)	4.7(6)
$r_E^d$ dipole	3.63(14)	3.9(2)	4.0(7)	4.4(8)
$r_M^d$ dipole	3.69(12)	4.00(18)	4.3(4)	4.9(6)
$r_E$ monopole	3.77(13)	4.31(19)	4.5(4)	5.1(6)
$r_M$ monopole	3.78(13)	4.07(18)	4.3(5)	4.8(8)
$r_E^d$ monopole	3.70(14)	3.9(3)	4.1(7)	4.5(8)
$r_M^d$ monopole	3.75(13)	4.09(19)	4.4(4)	5.0(6)

TABLE V. Neutron electromagnetic form factors and radii.

	$\kappa_1=0.152$	$\kappa_2=0.154$	$\kappa_3=0.156$	$\kappa_{cr}=0.1598(2)$
Mass $a$	1.09(3)	0.96(3)	0.84(3)	0.61(5)
$q^2 a^2$	0.067 58(6)	0.067 31(7)	0.066 95(10)	0.066 1(11)
$G_E(q^2)$	0.002(3)	0.006(7)	0.014(16)	0.02(2)
$G_M(q^2)$	-1.18(6)	-1.14(10)	-1.10(15)	-1.1(2)
$G_M(0)$	-1.37(7)	-1.36(11)	-1.33(18)	-1.3(2)
$G_E^d(q^2)$	-0.575(6)	-0.561(8)	-0.548(18)	-0.52(2)
$G_M^d(q^2)$	-0.85(5)	-0.84(7)	-0.85(8)	-0.85(13)
$G_M^d(0)$	-0.99(5)	-1.00(7)	-1.03(8)	-1.07(12)
$G_E^u(q^2)$	0.578(5)	0.568(10)	0.56(3)	0.54(4)
$G_M^u(q^2)$	-0.33(2)	-0.30(4)	-0.25(11)	-0.20(15)
$G_M^u(0)$	-0.38(3)	-0.35(5)	-0.29(14)	-0.25(17)
$r_M$ dipole	3.72(13)	3.95(19)	4.1(8)	4.6(6)
$r_E^d$ dipole	3.69(12)	4.00(18)	4.3(4)	4.9(6)
$r_E^u$ dipole	3.63(14)	3.9(2)	4.0(7)	4.4(8)
$r_M$ monopole	3.79(13)	4.0(2)	4.2(9)	4.6(7)
$r_E^d$ monopole	3.75(13)	4.09(19)	4.4(4)	5.0(6)
$r_E^u$ monopole	3.70(14)	3.9(3)	4.1(7)	4.5(8)

TABLE VI.  $\Lambda$  octet electromagnetic form factors and radii.

	$\kappa_1=0.152$	$\kappa_2=0.154$	$\kappa_3=0.156$	$\kappa_{cr}=0.1598(2)$
Mass $a$	1.09(3)	1.00(3)	0.92(3)	0.76(5)
$q^2 a^2$	0.067 58(6)	0.067 41(7)	0.067 20(7)	0.067 2(16)
$G_E(q^2)$	0.001 0(14)	-0.006(3)	-0.013(13)	-0.027(17)
$G_M(q^2)$	-0.59(3)	-0.54(4)	-0.50(5)	-0.42(8)
$G_M(0)$	-0.68(4)	-0.63(4)	-0.57(7)	-0.48(8)
$G_E^s(q^2)$	-0.287(3)	-0.288(3)	-0.290(4)	-0.292(8)
$G_M^s(q^2)$	-0.62(4)	-0.58(4)	-0.54(4)	-0.46(7)
$G_M^s(0)$	-0.72(4)	-0.67(5)	-0.62(5)	-0.52(7)
$G_E^l(q^2)$	0.288(3)	0.282(4)	0.277(13)	0.27(2)
$G_M^l(q^2)$	0.033(10)	0.034(16)	0.03(3)	0.04(4)
$G_M^l(0)$	0.038(14)	0.040(19)	0.04(3)	0.05(5)
$r_M$ dipole	3.72(13)	3.7(2)	3.7(3)	3.6(5)
$r_E^s$ dipole	3.70(13)	3.66(15)	3.6(2)	3.5(3)
$r_E^l$ dipole	3.65(13)	3.94(18)	4.2(4)	4.7(7)
$r_M$ monopole	3.79(13)	3.8(3)	3.8(5)	3.7(5)
$r_E^s$ monopole	3.77(13)	3.72(15)	3.7(2)	3.6(3)
$r_E^l$ monopole	3.72(14)	4.0(2)	4.3(6)	4.8(7)
$\Sigma^0 \rightarrow \Lambda$ transition				
$G_M(q^2)$	-1.03(5)	-1.06(6)	-1.08(10)	-1.12(15)
$G_M(0)$	-1.19(6)	-1.26(7)	-1.33(13)	-1.4(2)

TABLE VII.  $\Lambda$  common electromagnetic form factors and radii.

	$\kappa_1=0.152$	$\kappa_2=0.154$	$\kappa_3=0.156$	$\kappa_{cr}=0.1598(2)$
Mass $a$	1.09(3)	1.01(3)	0.92(3)	0.77(4)
$q^2 a^2$	0.067 58(6)	0.067 42(6)	0.067 22(8)	0.066 7(14)
$G_E(q^2)$	0.000 1(13)	-0.008(3)	-0.018(7)	-0.032(10)
$G_M(q^2)$	-0.57(6)	-0.54(7)	-0.50(9)	-0.44(13)
$G_M(0)$	-0.67(6)	-0.62(8)	-0.57(10)	-0.48(15)
$G_E^s(q^2)$	-0.289(3)	-0.290(4)	-0.293(5)	-0.295(10)
$G_M^s(q^2)$	-0.61(5)	-0.57(7)	-0.54(7)	-0.47(11)
$G_M^s(0)$	-0.71(6)	-0.66(7)	-0.61(9)	-0.52(9)
$G_E^l(q^2)$	0.288(3)	0.282(4)	0.275(8)	0.263(18)

TABLE VI. (Continued).

	$\kappa_1=0.152$	$\kappa_2=0.154$	$\kappa_3=0.156$	$\kappa_{cr}=0.1598(2)$
$G_M^I(q^2)$	0.037(14)	0.033(17)	0.03(2)	0.03(4)
$G_M^I(0)$	0.043(16)	0.04(2)	0.04(2)	0.04(4)
$r_M$ dipole	3.69(18)	3.7(3)	3.4(8)	3.4(8)
$r_E^S$ dipole	3.64(15)	3.58(18)	3.5(2)	3.3(3)
$r_E^I$ dipole	3.64(13)	3.95(15)	4.2(3)	4.8(5)
$r_M$ monopole	3.76(19)	3.7(3)	3.4(9)	3.4(10)
$r_E^S$ monopole	3.71(15)	3.64(16)	3.5(2)	3.4(3)
$r_E^I$ monopole	3.72(14)	4.04(19)	4.3(4)	4.9(7)
$\Sigma^0 \rightarrow \Lambda$ transition				
$G_M(q^2)$	-1.07(4)	-1.09(5)	-1.07(9)	-1.10(15)
$G_M(0)$	-1.24(5)	-1.30(6)	-1.32(11)	-1.4(2)

TABLE VIII.  $\Sigma^+$  electromagnetic form factors and radii.

	$\kappa_1=0.152$	$\kappa_2=0.154$	$\kappa_3=0.156$	$\kappa_{cr}=0.1598(2)$
Mass $a$	1.09(3)	1.01(3)	0.92(3)	0.76(4)
$q^2 a^2$	0.06758(6)	0.06742(7)	0.06721(8)	0.06731(14)
$G_E(q^2)$	0.862(8)	0.830(12)	0.791(18)	0.73(3)
$G_M(q^2)$	1.86(11)	1.89(15)	1.90(18)	1.9(3)
$G_M(0)$	2.16(12)	2.24(17)	2.3(2)	2.4(3)
$G_E^S(q^2)$	-0.289(3)	-0.290(3)	-0.293(5)	-0.296(9)
$G_M^S(q^2)$	0.165(12)	0.141(19)	0.12(4)	0.07(5)
$G_M^S(0)$	0.191(13)	0.16(2)	0.13(3)	0.08(6)
$G_E^U(q^2)$	1.151(11)	1.120(15)	1.08(3)	1.03(4)
$G_M^U(q^2)$	1.70(10)	1.74(14)	1.76(17)	1.8(3)
$G_M^U(0)$	1.97(11)	2.08(16)	2.2(2)	2.4(3)
$r_E$ dipole	3.70(13)	4.17(17)	4.7(2)	5.7(4)
$r_M$ dipole	3.71(13)	4.00(17)	4.4(2)	5.0(4)
$r_E^S$ dipole	3.63(14)	3.57(17)	3.4(2)	3.3(4)
$r_E^U$ dipole	3.69(12)	4.03(16)	4.4(2)	5.0(4)
$r_E$ monopole	3.77(13)	4.27(18)	4.9(3)	5.8(5)
$r_M$ monopole	3.78(13)	4.09(18)	4.5(3)	5.1(5)
$r_E^S$ monopole	3.70(14)	3.63(18)	3.5(2)	3.4(4)
$r_E^U$ monopole	3.75(13)	4.12(17)	4.5(2)	5.2(4)

TABLE IX.  $\Sigma^0$  electromagnetic form factors and radii.

	$\kappa_1=0.152$	$\kappa_2=0.154$	$\kappa_3=0.156$	$\kappa_{cr}=0.1598(2)$
Mass $a$	1.09(3)	1.01(3)	0.92(3)	0.76(4)
$q^2 a^2$	0.06758(6)	0.06742(7)	0.06721(8)	0.06674(13)
$G_E(q^2)$	-0.0012(14)	-0.0104(17)	-0.022(3)	-0.039(4)
$G_M(q^2)$	0.59(3)	0.58(4)	0.56(7)	0.54(9)
$G_M(0)$	0.68(4)	0.68(5)	0.68(7)	0.68(11)
$G_E^S(q^2)$	-0.289(3)	-0.290(3)	-0.293(5)	-0.296(10)
$G_M^S(q^2)$	0.165(12)	0.141(19)	0.12(4)	0.07(5)
$G_M^S(0)$	0.191(13)	0.16(2)	0.13(3)	0.08(6)
$G_E^I(q^2)$	0.288(2)	0.280(3)	0.271(5)	0.258(11)
$G_M^I(q^2)$	0.42(3)	0.44(3)	0.44(4)	0.45(6)
$G_M^I(0)$	0.49(3)	0.52(4)	0.54(5)	0.59(7)
$r_M$ dipole	3.72(13)	3.92(18)	4.2(3)	4.6(4)
$r_E^S$ dipole	3.63(14)	3.57(17)	3.4(2)	3.3(4)
$r_E^I$ dipole	3.69(12)	4.03(16)	4.4(2)	5.0(4)
$r_M$ monopole	3.79(13)	4.01(19)	4.3(3)	4.8(5)
$r_E^S$ monopole	3.70(14)	3.63(18)	3.5(2)	3.4(4)
$r_E^I$ monopole	3.75(13)	4.12(17)	4.5(2)	5.2(4)

TABLE X.  $\Sigma^-$  electromagnetic form factors and radii.

	$\kappa_1=0.152$	$\kappa_2=0.154$	$\kappa_3=0.156$	$\kappa_{cr}=0.1598(2)$
Mass $a$	1.09(3)	1.01(3)	0.92(3)	0.76(4)
$q^2 a^2$	0.067 58(6)	0.067 42(7)	0.067 21(8)	0.067 31(14)
$G_E(q^2)$	-0.864(8)	-0.850(11)	-0.835(15)	-0.81(3)
$G_M(q^2)$	-0.69(4)	-0.73(6)	-0.76(7)	-0.84(10)
$G_M(0)$	-0.79(5)	-0.88(6)	-0.95(8)	-1.11(11)
$G_E^s(q^2)$	-0.289(3)	-0.290(3)	-0.293(5)	-0.296(9)
$G_M^s(q^2)$	0.165(12)	0.141(19)	0.12(4)	0.07(5)
$G_M^s(0)$	0.191(13)	0.16(2)	0.13(3)	0.08(6)
$G_E^d(q^2)$	-0.575(6)	-0.560(7)	-0.542(11)	-0.51(2)
$G_M^d(q^2)$	-0.85(5)	-0.87(7)	-0.88(9)	-0.92(12)
$G_M^d(0)$	-0.99(5)	-1.04(8)	-1.09(10)	-1.18(15)
$r_E$ dipole	3.67(13)	3.88(16)	4.1(2)	4.5(3)
$r_M$ dipole	3.67(12)	4.14(16)	4.6(2)	5.4(3)
$r_E^s$ dipole	3.63(14)	3.57(17)	3.4(2)	3.3(4)
$r_E^d$ dipole	3.69(12)	4.03(16)	4.4(2)	5.0(4)
$r_E$ monopole	3.74(13)	3.96(17)	4.2(2)	4.6(3)
$r_M$ monopole	3.74(15)	4.24(17)	4.7(2)	5.6(3)
$r_E^s$ monopole	3.70(14)	3.63(18)	3.5(2)	3.4(4)
$r_E^d$ monopole	3.75(13)	4.12(17)	4.5(2)	5.2(4)

TABLE XI.  $\Xi^0$  electromagnetic form factors and radii.

	$\kappa_1=0.152$	$\kappa_2=0.154$	$\kappa_3=0.156$	$\kappa_{cr}=0.1598(2)$
Mass $a$	1.09(3)	1.05(3)	1.00(3)	0.91(4)
$q^2 a^2$	0.067 58(6)	0.067 50(6)	0.067 40(6)	0.067 2(14)
$G_E(q^2)$	0.002(3)	-0.012(5)	-0.029(14)	-0.06(2)
$G_M(q^2)$	-1.18(6)	-1.17(7)	-1.15(8)	-1.13(10)
$G_M(0)$	-1.37(7)	-1.36(8)	-1.35(8)	-1.33(11)
$G_E^s(q^2)$	-0.575(6)	-0.576(6)	-0.578(5)	-0.579(12)
$G_M^s(q^2)$	-0.85(5)	-0.82(5)	-0.78(6)	-0.72(6)
$G_M^s(0)$	-0.99(5)	-0.95(6)	-0.90(6)	-0.83(7)
$G_E^u(q^2)$	0.578(5)	0.564(8)	0.548(13)	0.52(3)
$G_M^u(q^2)$	-0.33(2)	-0.35(3)	-0.37(4)	-0.40(6)
$G_M^u(0)$	-0.38(3)	-0.42(3)	-0.45(5)	-0.51(7)
$r_M$ dipole	3.72(13)	3.78(15)	3.84(18)	3.9(3)
$r_E^s$ dipole	3.69(12)	3.67(13)	3.64(14)	3.57(18)
$r_E^u$ dipole	3.63(14)	3.94(19)	4.3(3)	4.9(5)
$r_M$ monopole	3.79(13)	3.85(16)	3.9(2)	4.1(4)
$r_E^s$ monopole	3.75(13)	3.74(14)	3.70(15)	3.63(19)
$r_E^u$ monopole	3.70(14)	4.02(18)	4.4(3)	5.0(6)

TABLE XII.  $\Xi^-$  electromagnetic form factors and radii.

	$\kappa_1=0.152$	$\kappa_2=0.154$	$\kappa_3=0.156$	$\kappa_{cr}=0.1598(2)$
Mass $a$	1.09(3)	1.05(3)	1.00(3)	0.91(4)
$q^2 a^2$	0.067 58(6)	0.067 50(6)	0.067 40(6)	0.067 2(14)
$G_E(q^2)$	-0.864(8)	-0.858(9)	-0.852(12)	-0.844(17)
$G_M(q^2)$	-0.69(4)	-0.64(5)	-0.60(6)	-0.53(6)
$G_M(0)$	-0.79(5)	-0.74(5)	-0.68(6)	-0.58(8)
$G_E^s(q^2)$	-0.575(6)	-0.576(6)	-0.578(5)	-0.579(12)
$G_M^s(q^2)$	-0.85(5)	-0.82(5)	-0.78(6)	-0.72(6)
$G_M^s(0)$	-0.99(5)	-0.95(6)	-0.90(6)	-0.83(7)

TABLE XII. (Continued).

	$\kappa_1=0.152$	$\kappa_2=0.154$	$\kappa_3=0.156$	$\kappa_{cr}=0.159\ 8(2)$
$G_E(q^2)$	-0.289(3)	-0.282(4)	-0.274(8)	-0.262(13)
$G_M^d(q^2)$	0.165(12)	0.175(14)	0.18(2)	0.20(3)
$G_M^d(0)$	0.191(13)	0.208(16)	0.22(3)	0.25(4)
$r_E$ dipole	3.67(13)	3.76(14)	3.86(18)	4.0(2)
$r_M$ dipole	3.67(12)	3.55(18)	3.4(3)	3.2(3)
$r_E^s$ dipole	3.69(12)	3.67(13)	3.64(14)	3.57(18)
$r_E^d$ dipole	3.63(14)	3.94(19)	4.3(3)	4.9(5)
$r_E$ monopole	3.74(13)	3.84(15)	3.93(19)	4.1(3)
$r_M$ monopole	3.74(15)	3.61(19)	3.5(4)	3.3(4)
$r_E^s$ monopole	3.75(13)	3.74(14)	3.70(15)	3.63(19)
$r_E^d$ monopole	3.70(14)	4.02(18)	4.4(3)	5.0(6)

TABLE XIII. A singlet electromagnetic form factors and radii.

	$\kappa_1=0.152$	$\kappa_2=0.154$	$\kappa_3=0.156$	$\kappa_{cr}=0.159\ 8(2)$
Mass $a$	1.14(20)	0.98(21)	0.80(24)	0.5(2)
$q^2 a^2$	0.067 7(3)	0.067 4(4)	0.066 8(8)	0.066 3(11)
$G_E(q^2)$	0	-0.005(3)	-0.010(8)	-0.017(11)
$G_M(q^2)$	0	0.04(5)	0.07(10)	0.14(18)
$G_M(0)$	0	0.05(6)	0.10(13)	0.2(2)
$G_E^s(q^2)$	-0.298(11)	-0.296(13)	-0.293(16)	-0.29(2)
$G_M^s(q^2)$	-0.17(12)	-0.15(12)	-0.12(12)	-0.08(14)
$G_M^s(0)$	-0.19(13)	-0.16(13)	-0.13(14)	-0.09(16)
$G_E^l(q^2)$	0.298(11)	0.292(15)	0.28(2)	0.27(3)
$G_M^l(q^2)$	0.17(12)	0.19(14)	0.19(19)	0.2(3)
$G_M^l(0)$	0.19(13)	0.22(16)	0.2(2)	0.3(3)
$r_E$ dipole	0	0.68(15)	1.0(3)	1.3(3) <sup>a</sup>
$r_M$ dipole	0	7(5)	7(9)	7(3) <sup>a</sup>
$r_E^s$ dipole	3.2(5)	3.3(6)	3.4(8)	3.6(10)
$r_E^l$ dipole	3.2(5)	3.5(7)	3.9(9)	4.4(13)
$r_E$ monopole	0	0.68(15)	1.0(3)	1.3(3) <sup>a</sup>
$r_M$ monopole	0	8(3)	7(10)	7(3) <sup>a</sup>
$r_E^s$ monopole	3.2(5)	3.3(7)	3.5(8)	3.7(11)
$r_E^l$ monopole	3.2(5)	3.6(7)	4.0(1)	4.5(14)

<sup>a</sup>Values obtained using extrapolated electric and magnetic moments.

TABLE XIV. Proton interpolating field  $\epsilon^{abc}(u^a T C \gamma_\rho u^b) \gamma_5 \gamma^\rho d^c$ .

	$\kappa_1=0.152$	$\kappa_2=0.154$	$\kappa_3=0.156$	$\kappa_{cr}=0.159\ 8(2)$
Mass $a$	1.09(3)	0.96(3)	0.82(3)	0.57(6)
$q^2 a^2$	0.067 58(6)	0.067 31(8)	0.066 87(12)	0.066 1(12)
$G_E(q^2)$	0.863(11)	0.838(14)	0.80(3)	0.75(4)
$G_M(q^2)$	1.92(11)	1.89(13)	1.79(16)	1.7(2)
$G_M(0)$	2.23(11)	2.25(13)	2.20(15)	2.2(3)
$G_E^d(q^2)$	-0.289(3)	-0.283(6)	-0.281(17)	-0.27(2)
$G_M^d(q^2)$	0.176(19)	0.16(3)	0.13(7)	0.10(10)
$G_M^d(0)$	0.20(2)	0.19(3)	0.15(8)	0.13(11)
$G_E^u(q^2)$	1.151(13)	1.12(2)	1.08(4)	1.03(7)
$G_M^u(q^2)$	1.74(10)	1.72(11)	1.65(12)	1.6(2)
$G_M^u(0)$	2.03(10)	2.07(12)	2.04(12)	2.1(2)
$r_E$ dipole	3.68(16)	4.1(2)	4.6(5)	5.3(6)
$r_M$ dipole	3.73(15)	4.1(2)	4.4(5)	5.0(7)
$r_E^d$ dipole	3.63(15)	3.9(3)	4.0(7)	4.4(10)
$r_E^u$ dipole	3.68(15)	4.0(2)	4.4(4)	5.0(6)
$r_E$ monopole	3.75(17)	4.2(3)	4.7(5)	5.4(7)
$r_M$ monopole	3.81(16)	4.2(2)	4.5(6)	5.1(8)
$r_E^d$ monopole	3.70(16)	4.0(3)	4.1(8)	4.5(11)
$r_E^u$ monopole	3.74(16)	4.1(2)	4.6(5)	5.2(6)

- <sup>1</sup>M. Creutz, L. Jacobs, and C. Rebbi, Phys. Rep. **95**, 201 (1983), and references therein.
- <sup>2</sup>M. A. Shifman, A. I. Vainshtein, and Z. I. Zakharov, Nucl. Phys. **B147**, 385 (1979); **B147**, 448 (1979).
- <sup>3</sup>W. Wilcox and R. M. Woloshyn, Phys. Rev. Lett. **54**, 2653 (1985); R. M. Woloshyn and A. M. Kobos, Phys. Rev. D **33**, 222 (1986); R. M. Woloshyn, *ibid.* **34**, 605 (1986).
- <sup>4</sup>T. Draper, R. M. Woloshyn, W. Wilcox, and K. F. Liu, Nucl. Phys. **B318**, 319 (1989); T. Draper, R. M. Woloshyn, W. Wilcox, and K. F. Liu, in *Field Theory on the Lattice*, proceedings of the International Symposium, Seillac, France, 1987, edited by A. Billoire *et al.* [Nucl. Phys. B (Proc. Suppl.) **4**, 524 (1988)].
- <sup>5</sup>G. Martinelli and C. T. Sachrajda, Nucl. Phys. **B306**, 865 (1988).
- <sup>6</sup>G. Martinelli and C. T. Sachrajda, Nucl. Phys. **B316**, 355 (1989).
- <sup>7</sup>T. Draper, R. M. Woloshyn, and K. F. Liu, Phys. Lett. B **234**, 121 (1990).
- <sup>8</sup>H. G. Dosch, M. Jamin, and S. Narison, Phys. Lett. B **220**, 251 (1989), and references therein.
- <sup>9</sup>Y. Chung, H. G. Dosch, M. Kremer, and D. Schall, Nucl. Phys. **B197**, 55 (1982).
- <sup>10</sup>J. Sakurai, *Advanced Quantum Mechanics* (Addison-Wesley, Reading, 1967).
- <sup>11</sup>See, for example, B. L. Ioffe, Nucl. Phys. **B188**, 317 (1981).
- <sup>12</sup>C. Bernard, T. Draper, G. Hockney, and A. Soni, in *Lattice Gauge Theory: A Challenge in Large-Scale Computing*, proceedings of the NATO Advanced Study Institute, Wuppertal, West Germany, 1985, edited by B. Bunk, K. H. Mutter, and K. Schilling, NATO ASI Series B: Physics, Vol. 140 (Plenum, New York, 1986).
- <sup>13</sup>C. Bernard, in *Gauge Theory on a Lattice*, edited by C. Zachos, W. Celmaster, E. Kovacs, and D. Sivers (National Technical Information Service, Springfield, 1984).
- <sup>14</sup>T. Draper, R. M. Woloshyn, W. Wilcox, and K. F. Liu, in *Lattice '88*, proceedings of the International Symposium, Batavia, Illinois, 1988, edited by P. MacKenzie and A. Kronfeld [Nucl. Phys. B (Proc. Suppl.) **9** (1989)].
- <sup>15</sup>N. Cabibbo and E. Marinari, Phys. Lett. **119B**, 387 (1982).
- <sup>16</sup>This proved sufficient to achieve good statistical independence of the ensemble. An examination of a number of observables, configuration by configuration, revealed no apparent long-range correlation in our gauge configuration sample.
- <sup>17</sup>B. Efron, SIAM Rev. **21**, 460 (1979); S. Gottlieb, P. B. MacKenzie, H. B. Thacker, and D. Weingarten, Nucl. Phys. **B263**, 704 (1986).
- <sup>18</sup>Particle Data Group, G. P. Yost *et al.*, Phys. Lett. B **204**, 1 (1988).
- <sup>19</sup>This interval differs slightly from that used in Ref. 7; however, the results agree within uncertainties.
- <sup>20</sup>J. Bernstein, *Elementary Particles and Their Currents* (Freeman, San Francisco 1968).
- <sup>21</sup>G. G. Simon *et al.*, Z. Naturforsch **35a**, 1 (1980); O. Dumbrajs *et al.*, Nucl. Phys. **B216**, 277 (1983).
- <sup>22</sup>N. Barik, S. N. Jena, and D. P. Rath, Phys. Rev. D **41**, 1568 (1990). We have corrected the value of the calculated  $\Sigma^-$  magnetic moment given in Table I of their paper.
- <sup>23</sup>J. Kunz and P. J. Mulders, Phys. Rev. D **41**, 1578 (1990).
- <sup>24</sup>R. D. Carlitz, S. D. Ellis, and R. Savit, Phys. Lett. **68B**, 433 (1977).
- <sup>25</sup>The simple-quark-model ratio of 8 may be recovered in lattice calculations at small values of  $\kappa$  where the quarks are more massive. For example, at  $\kappa=0.130$  the ratio is reduced to 8.52(17). The ratio increases as the quarks become lighter.
- <sup>26</sup>C. B. Chiu, J. Pasupathy, and S. J. Wilson, Phys. Rev. D **33**, 1961 (1986); **36**, 1553 (1987).
- <sup>27</sup>S. Nozawa and D. B. Leinweber, Phys. Rev. D **42**, 3567 (1990).
- <sup>28</sup>J. Lach, in *High Energy Spin Physics*, proceedings of the VIII International Symposium, Minneapolis, Minnesota, 1988, edited by K. Heller, AIP Conf. Proc. No. 187 (AIP, New York, 1989).